Supporting Information

Yuhan Mei and N. Aaron Deskins*

Department of Chemical Engineering, Worcester Polytechnic Institute, Worcester, MA 01609

E-mail: nadeskins@wpi.edu

1 Further Information on the Density Functional Theory Simulations

We used projector augmented wave (PAW) pseudopotentials[1,2] to represent core electrons. We calculated adsorption energies using Rh pseudopotentials with either 9 or 15 valence electrons, as found in Table S1. These results confirm that 9 valence electrons are sufficient for modeling surface chemistry over Rh (111).

Table S1: Comparison of adsorption energies using different pseudopotentials for Rh. We compared pseudopotentials with 9 valence electrons and 15 valence electrons.

	ΔE_{ads} (eV)	
	Rh - 9 e^-	Rh - 15 e^-
*CH_3	-1.81	-1.79
*CH_2	-4.13	-4.12
*CH	-6.67	-6.68
*CO	-1.93	-1.93

Figure S1 shows the slab model we used in the current work. To find stable configurations of the adsorbed species in vacuum, we modeled several different geometries for every adsorbed species. Adsorbates were initially placed above the surface with atoms of the adsorbates

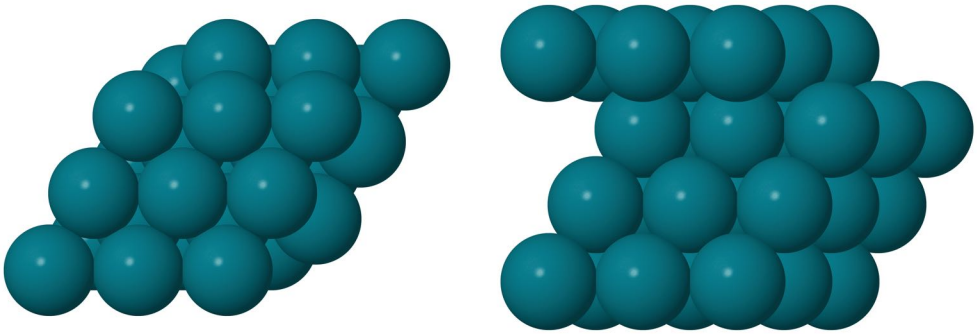

Figure S1: The slab model used in the work to represent the Rh (111) surface. The slab was a (3x3) slab with four layers, the bottom two layers being frozen.

at different fcc, hcp, top and bridge sites on the Rh(111) surface. These structures were then allowed to relax. The adsorption of larger molecules (e.g. CH_3CH_2OH, CH_3CH_2O, CH_2CH_2O, CH_3CO, CH_2CO, CHCO, CH_3COOH) can involve multiple interactions with the surface. For example, *CHCO can have both of the C atoms interacting with Rh atoms on the surface. After geometry optimization, we took the structure with the lowest energy as the most stable configuration.

The most stable geometries from vacuum calculations were used as the starting point for explicit solvation calculations, as shown in Figure S2. We then added one solvent molecule to interact with the surface species in what we call the explicit model, while the explicit+ model contained two solvent molecules. We took the most stable explicit solvent configurations and then applied implicit solvation for these hybrid calculations. Figure S2 shows ethanol adsorbed in these various solvent environments. For the explicit solvation calculations, four different initial geometries were simulated for each adsorbate. For adsorbates that have both O and H atoms (like ethanol, CH_3CH_2O, CH_2CH_2O, CH_2OH, CH_2O, CH_xCO, OH) , two initial geometries had the H atom of the solvent molecule initially placed to interact with the O atom of the adsorbate, as shown in Figure S3. In one of these two cases, the solvent molecule also interacted with the metal surface, while in the other case the solvent molecule

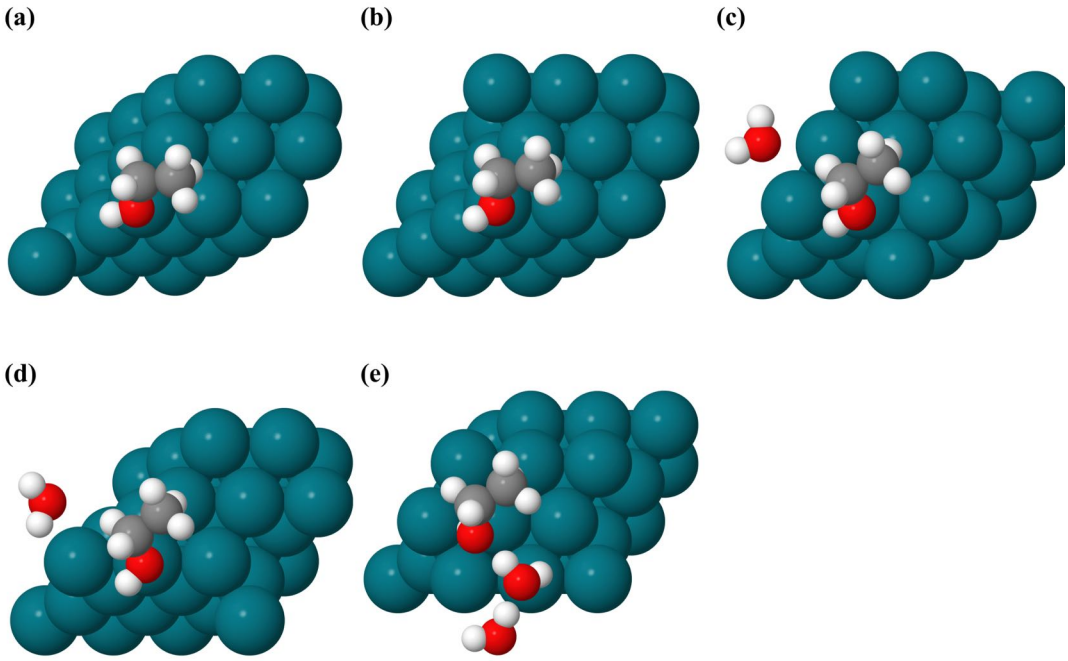

Figure S2: Geometries of ethanol adsorbed on the Rh(111) surface in (a) vacuum, (b) implicit water, (c) explicit water, (d) hybrid water, and (e) explicit+ water.

interacted weakly with the surface due to a long solvent-metal distance. For the other two initial geometries, the O atom of the solvent atom was initially arranged to interact with different H atoms of the adsorbate. Figure S3 shows an example of the initial structures of adsorbed ethanol in explicit water solvation.

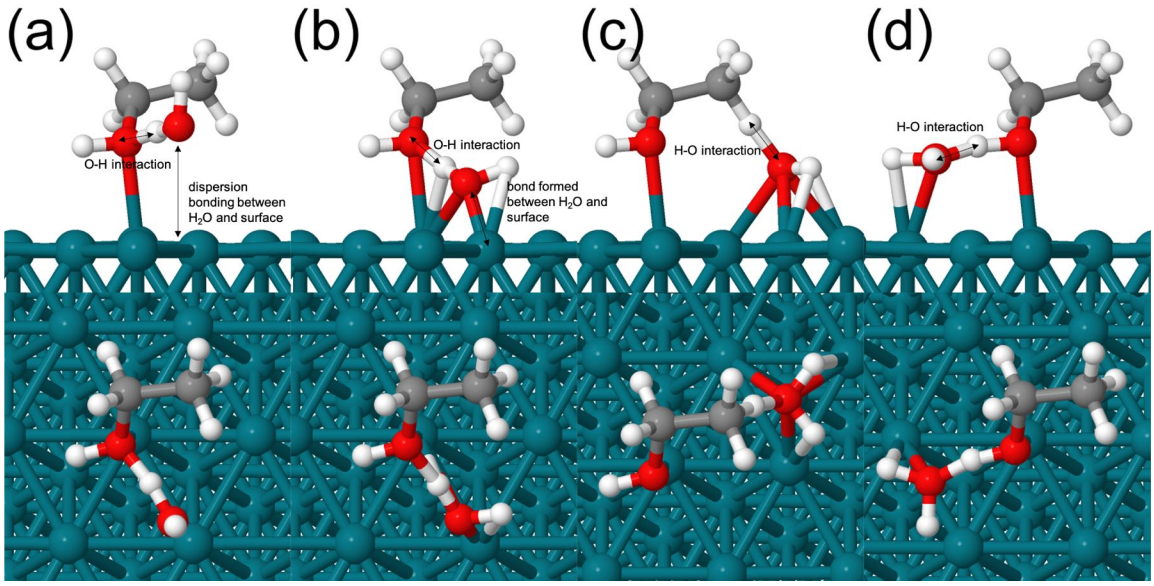

Figure S3: Initial geometries of ethanol adsorbed on the Rh(111) surface in explicit water solvation. (a) and (b) show the first two initial structures with solvent interacting with O in adsorbate; (c) and (d) show the other two initial structures with solvent interacting with H in adsorbate.

For smaller adsorbates that only had either O or H atoms (e.g., CH_x, CO, and H), four different initial geometries were also considered to find the most stable adsorption structures. The first two initial geometries involved hydrogen bonding, while the second two cases did not. For the first two geometries of CH_x (Figure S4), the solvent molecules were initially placed to interact with CH_x via the adsorbate's H atom, forming hydrogen bonds with the solvent. As for CO (Figure S5), the solvent molecules were initially placed to interact with the O atom in CO, forming hydrogen bonds in the first two geometries. For the first two initial structures involving CH_x and CO adsorbates, as with larger adsorbates, we considered initial geometries where the solvent molecule interacted with the adsorbate, but could be placed to either be bound to the surface or had weak interaction with the Rh surface (i.e. placed far above the surface). The solvent molecules interacted with the C atoms through C-H and C-O bonding for the other two cases involving CH_x and CO adsorbates. With adsorbed H (Figure S6), the most stable optimized geometry in vacuum was chosen as the starting point (with a H atom placed at a fcc site). For the first three initial geometries

the solvent molecules were initially placed at different adsorption sites on the metal surface (hcp, atop, bridge) to interact with the adsorbed H and form a hydrogen bond, while the solvent was placed to weakly interact with the surface for the fourth initial geometries. The configuration with the lowest energy among the four optimized geometries for a given adsorbate was considered the most stable structure for each explicit solvation/adsorbate system.

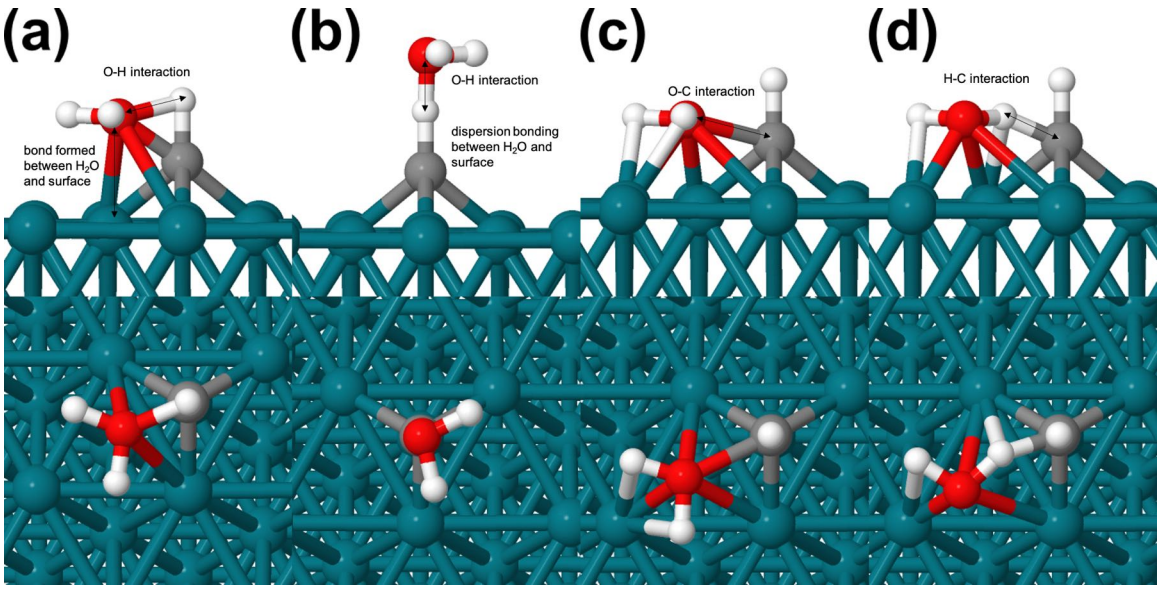

Figure S4: Initial geometries of CH adsorbed on the Rh(111) surface in explicit water solvation. (a) and (b) show the first two initial structures with solvent interacting with H in adsorbate; (c) and (d) show the other two initial structures with solvent forming O-C and H-C interactions.

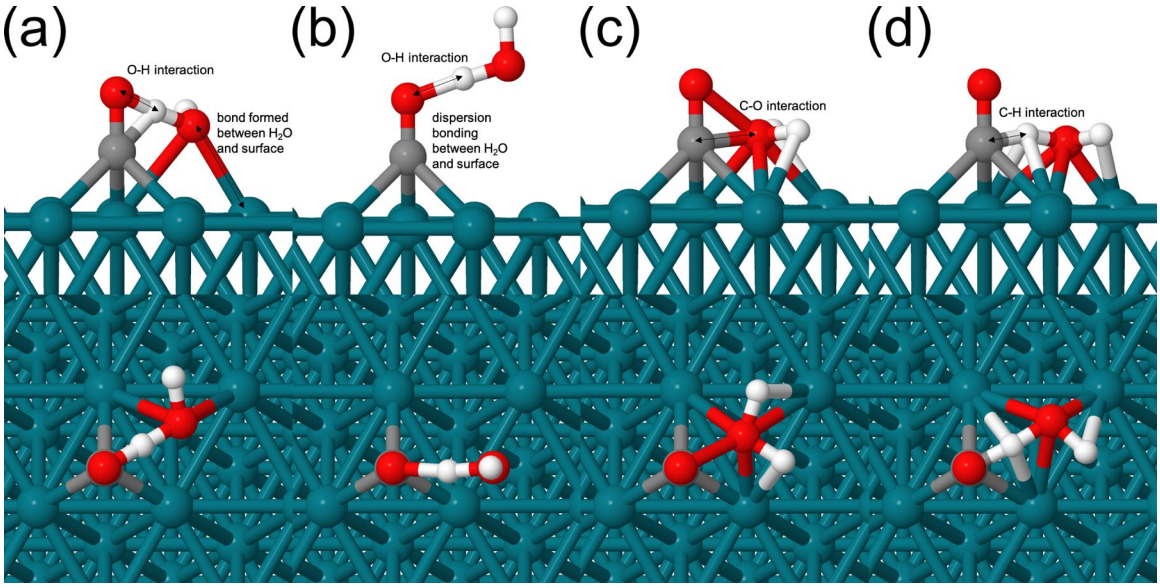

Figure S5: Initial geometries of CO adsorbed on the Rh(111) surface in explicit water solvation. (a) and (b) show the first two initial structures with solvent interacting with O in adsorbate; (c) and (d) show the other two initial structures with solvent forming C-O and C-H interactions.

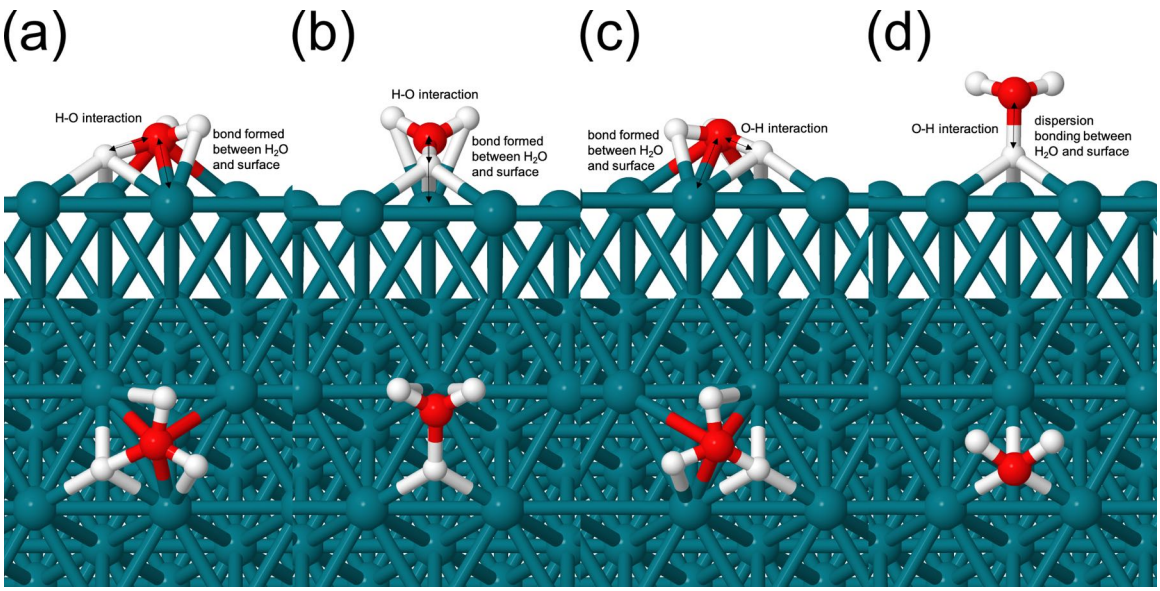

Figure S6: Initial geometries of H adsorbed on the Rh(111) surface in explicit water solvation. (a), (b) and (c) show the first three initial structures with solvent adsorbed at different sites on surface; (d) shows the initial structure with solvent had no surface interaction.

Different initial structures were modeled for *solv with solvent molecules adsorbed at different sites. For the explicit method, the solvent molecule was modeled at fcc, hcp,

atop, and bridge sites on the Rh(111) surface, and the one that had the lowest energy after geometry optimization was chosen as the most stable structure for the *solv configuration. For explicit+ solvation, the most stable structure of the solvent from the explicit method was chosen as the starting point and the second solvent molecule was modeled to interact with the first solvent molecule in different initial geometries. Two initial geometries had the H atom of the solvent molecule initially placed to interact with the O atom of the adsorbate. In one of these two cases, the solvent molecule also interacted with the metal surface, while in the other case the solvent molecule interacted only with the adsorbate molecule. For the other two initial geometries, the O atom of the solvent atom was initially arranged to interact with different H atoms of the adsorbate. The optimized geometries of *solv for water and ethanol are shown in Figure S7. A similar structure for two water molecules over Rh(111) was found by other DFT papers.[3–6]

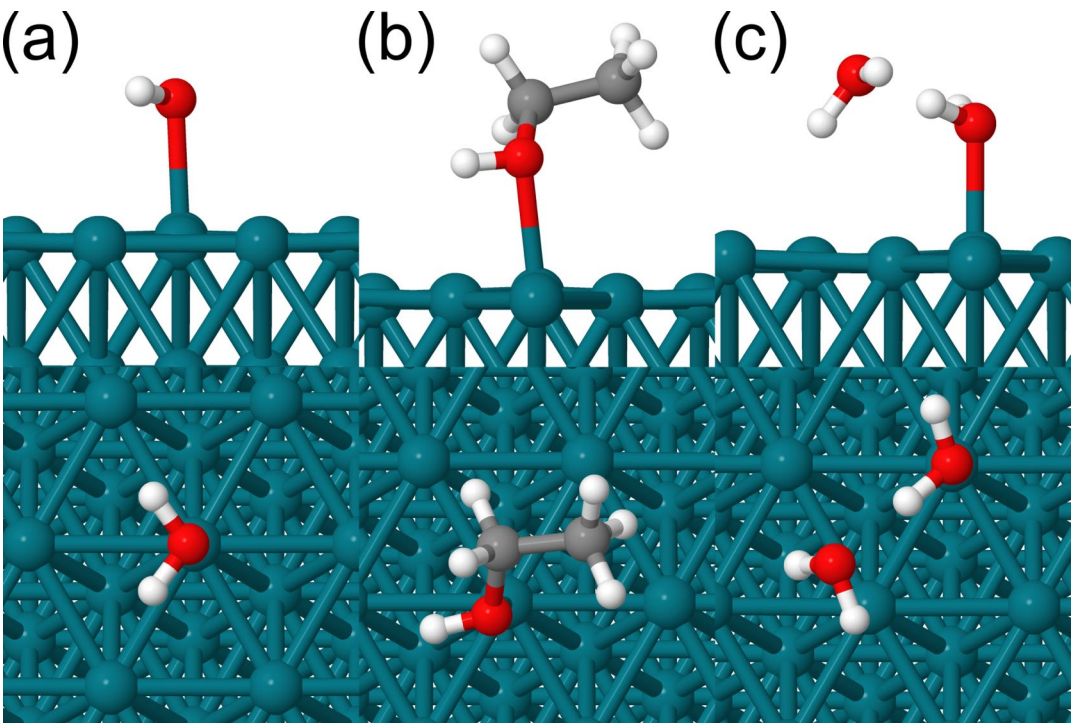

Figure S7: Optimized geometries of *solv on the Rh(111) surface for explicit and explicit+ solvation methods. For explicit: (a) water, (b) ethanol; for explicit+: (c) water-water.

2 Validating Our Calculations in Vacuum

One of the first steps of our work was to run calculations in vacuum to compare with literature and validate our approach. Several initial geometries were considered, and after geometry optimization the structures with the lowest energies were considered as the preferable configurations. Adsorption energies of reactants and intermediates involved in C-C and C-H bond scission and C-O bond formation relevant to ethanol oxidation were calculated over the Rh(111) surface and are listed in Table S2. Figure S8 shows geometries of adsorbed species on the Rh(111) surface in vacuum. The geometries of adsorbed CH_3CH_2OH, CH_2OH, CH_3CO and CH_3COOH on the Rh(111) surface occupied atop sites, and CH_2OH and CH_3CO formed bridge structures with a C and O atom bonding to the metal atoms. CH_3CH_2O, CH_2CO, CO, H and OH adsorbed at fcc sites on the metal surface while CH_3, CH_2, and CH occupied the hcp sites. CH_2CH_2O, CH_2O and CHCO adsorbed at the bridge sites and CHCO formed a bridge structure with both the C atoms bonding to the metal atoms. Reaction energies are listed in Table S3, which shows consistent agreement with literature values. Thus, both the adsorption and reaction energy results agree well with literature values[7–14] and demonstrate that our approach is acceptable.

Table S2: Comparison of our calculated adsorption energies of surface species on Rh(111) in vacuum with literature values.

ΔE_{ads} (eV)		
	This work	Literature values
*CH_3CH_2OH	-0.35	-0.46;[9] -0.51;[8] -0.28[7]
*CH_3CH_2O	-2.30	-2.30[8]
*CH_2CH_2O	-1.18	-1.29[8]
*CH_2OH	-2.08	-1.74;[7] -2.27[12]
*CH_2O	-0.85	-0.68;[7] -1.07[12]
*CH_3CO	-2.38	-2.41[7]
*CH_2CO	-1.40	-1.41[8]
*CHCO	-3.39	-3.32[8]
*CH_3	-1.81	-1.90;[7] -1.97;[8] -1.32;[10]
*CH_2	-4.13	-4.14;[7] -4.15[8]
*CH	-6.78	-6.62;[7] -6.55[8]
*CO	-1.92	-1.93;[8] -2.04;[10] -1.77[7]
*H	-2.78	-2.79;[8] -2.79;[10] -2.74;[7] 2.79[11]
*OH	-3.06	-3.19[13]

Table S3: Comparison of our calculated reaction energies on Rh(111) in vacuum with literature values.

ΔE_{rxn} (eV)		
	this work	literature value
*CH_3CH_2OH + * → *CH_3 + *CH_2OH	0.50	0.71[14]
*CH_3CH_2O + * → *CH_3 + *CH_2O	0.46	0.55[14]
*CH_2CH_2O + * → *CH_2 + *CH_2O	0.03	0.34[14]
*CH_3CO + * → *CH_3 + *CO	-0.26	-0.03[14]
*CH_2CO + * → *CH_2 + *CO	-0.60	-0.33;[8] -0.18[14]
*CHCO + * → *CH + *CO	-0.98	-0.74;[8] -0.66[14]
*CH_3CO + * → *CH_2CO + *H	0.20	0.17[14]
*CH_2CO + * → *CHCO + *H	-0.13	0.07;[14] -0.05[8]
*CH_3CO + *OH → *CH_3COOH + *	-0.20	-0.27[13]

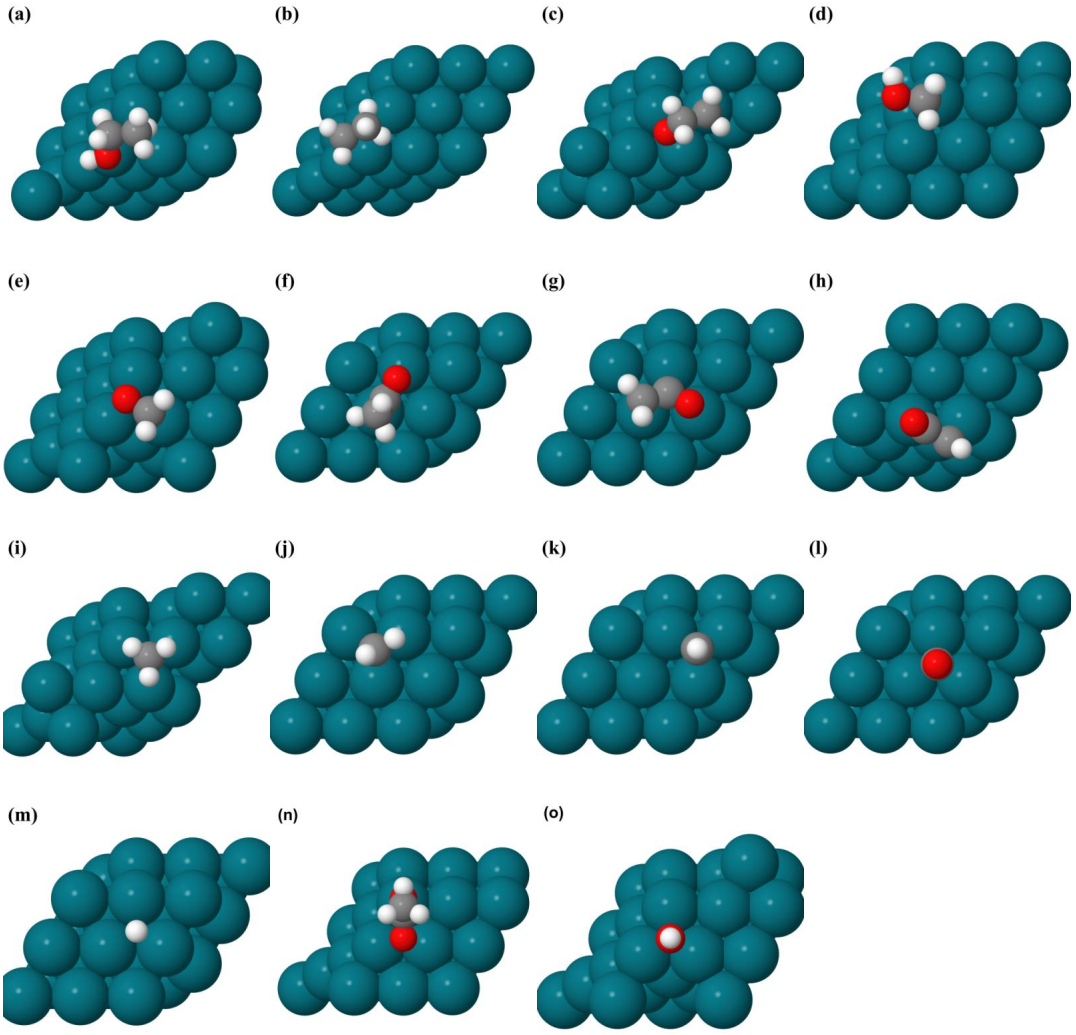

Figure S8: Geometries of ethanol components adsorbed on Rh(111) surfaces in the vacuum phase: (a)ethanol (b)CH_3CH_2O (c)CH_2CH_2O (d)CH_2OH (e)CH_2O (f)CH_3CO (g)CH_2CO (h)CHCO (i)CH_3 (j)CH_2 (k)CH (l)CO (m)H (n)CH_3COOH (o)OH

3 Comparison of Activation Energies using BEP Scaling Relationships

BEP correlations can estimate activation energies of dissociation based on the reaction energies through the following formulas (either in vacuum or implicit solvation):

$$\Delta E_{diss} = E(*A) + E(*B) - 2E(*) - E(AB(gas)). \tag{S1}$$

$$E_{TS} = \gamma \Delta E_{diss} + \xi. \tag{S2}$$

$$E_a = E_{TS} - \Delta E_{ads}(AB). \tag{S3}$$

Bond formation (i.e. C-O formation) is the opposite of bond breaking, and by calculating transition states of C-O breaking we are able to determine activation energies of the reverse process, or CO bond formation. We estimated activation energies of C-O bond formation based on C-O bond cleavage using the following formulas.

$$E_a(C - Oformation) = E_{TS} - \Delta E_{diss}. \tag{S4}$$

With explicit solvent, we have the following:[15,16]

$$E_a^{sol} = E_a^{vac} + (\Delta E_{rxn}^{sol} - \Delta E_{rxn}^{vac}). \tag{S5}$$

In the above equations, ΔE_{diss} is the dissociation energy and E_{TS} is the transition state energy. The variables Δ and ξ are fitted parameters.

We calculated the activation energies using the scaling relationship parameters from both Wang et al.'s[17,18] and Schweitzer et al.'s[19] work (Table S4). The calculated activation energies for C-C bond cleavage using these two different sets of parameters were similar, but the activation energies for C-H bond scission with Wang's parameters were closer to the values in previous work.[8,14] We note that these results used electronic reaction energies, rather

than free energies. However, in the case of implicit solvation, VASPsol reports solvation free energies in addition to electronic energies. These solvation free energies were small, as Figure S9 shows. Such solvation energies are defined as the difference in implicit and vacuum calculation energies.The average solvation energy was -0.06 eV in water and -0.02 eV in ethanol. Similar to previous work,[19] we assumed $G_{sol} \sim E_{sol}$. Furthermore, this previous work also used BEP relations with implicit solvation energies. This may introduce an error in the calculations, but since solvation energies using implicit solvation were so small, the error is minimal. Thus, with implicit solvation we used the electronic and solvation free energies when calculating activation energies with BEP relations.

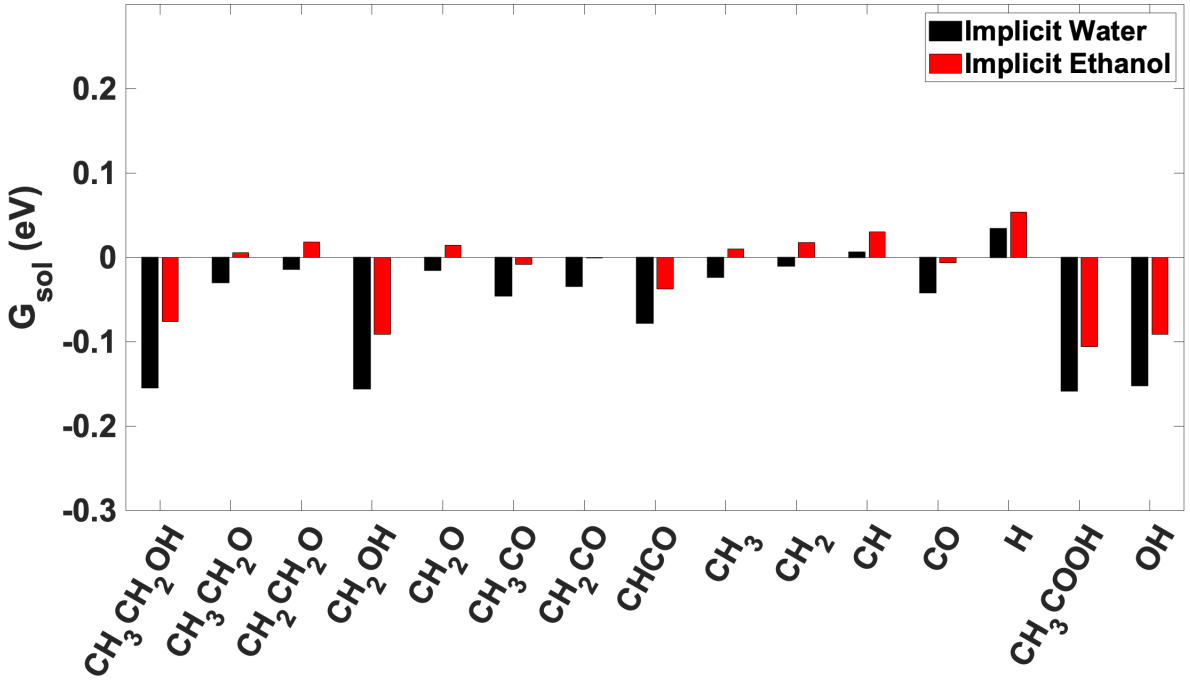

Figure S9: Calculated solvation free energies of select adsorbed molecules using implicit solvation in water or ethanol solvents. Results are obtained as the difference in energies between vacuum and implicit calculations.

Our calculated activation energies for CH_3CO and CH_2CO dehydrogenation in the vacuum were 1.18 and 0.88 eV using Wang's parameters, and 0.39 and 0.29 eV using Schweitzer's parameters. In previous literature involving transition state calculations, the activation energies for C-H scission in CH_3CO and CH_2CO were reported to be 1.47 and 0.83 eV,[14] while

another paper[8] reported a C-H scission activation energy for CH_2CO to be 0.66 eV. We therefore decided to use the γ and ξ parameters from Wang et al.'s work.[17,18]

Table S4: Our calculated activation energies (using two different correlations[17–19]) for C-C and C-H bond scission reactions on Rh(111) in vacuum. Also shown are literature values for comparison.

	E_{act} (eV)		
	Wang et al.[17,18]	Schweitzer et al.[19]	Literature values
$*CH_3CH_2OH + * \rightarrow *CH_3 + *CH_2OH$	2.02	1.91	2.97;[14] 3.20[8]
$*CH_3CH_2O + * \rightarrow *CH_3 + *CH_2O$	2.52	2.33	2.98;[14]2.93[8]
$*CH_2CH_2O + * \rightarrow *CH_2 + *CH_2O$	1.74	1.74	1.57;[14] 1.01[8]
$*CH_3CO + * \rightarrow *CH_3 + *CO$	2.22	1.78	1.61[14]
$*CH_2CO + * \rightarrow *CH_2 + *CO$	2.89	1.30	1.17;[8] 1.54[14]
$*CHCO + * \rightarrow *CH + *CO$	1.72	1.46	0.65;[8] 0.69[14]
$*CH_3CO + * \rightarrow *CH_2CO + *H$	1.19	0.40	1.47[14]
$*CH_2CO + * \rightarrow *CHCO + *H$	0.88	0.30	0.83;[14] 0.66[8]

4 Details on the Bond-Additivity Method

We followed previous work[20,21] to predict the aqueous-phase adsorption enthalpies on Rh(111) surfaces at 298.15 K and 1 atm:

$$\Delta H^{\circ}_{ads,aq,A/surface} = \Delta H^{\circ}_{ads,vac,A/surface}$$
$$-n(\Delta H^{\circ}_{ads,vac,water/surface} + \Delta H^{\circ}_{vap}) + 1/2\Delta H_{Solv,A} + \gamma_{water(liq)}\sigma_A. \quad \text{(S6)}$$

In the above equation, $\Delta H^{\circ}_{ads,aq,A/surface}$ is the adsorption enthalpy of species A adsorbed onto a Rh(111) surface in the presence of aqueous phase at standard conditions (298.15 K and 1 atm). $\Delta H^{\circ}_{ads,vac,A/surface}$ is the adsorption enthalpy of species A adsorbed onto Rh(111) surface in vacuum, and $\Delta H^{\circ}_{ads,vac,water/surface}$ is the adsorption enthalpy of a water molecule in vacuum. Both these values are derived from DFT calculations. The number of water molecules displaced upon adsorption of A is represented by n. The value n is calculated as $\frac{saturation\ coverage\ of\ water}{saturation\ coverage\ of\ the\ adsorbates}$. The saturation coverage of water on Pt(111) surface was reported to be 0.72 ML.[22] Since the saturation coverage is not known for water on

the Rh(111) surface, as indicated in Akinola et al.'s work,[20] we assumed that the saturation water coverage on Rh(111) was the same for Pt(111), similar to Akinola et al. The value of n we used corresponded to an adsorbate coverage of 1/9 ML, based on the size of our simulation cell with one adsorbate. Le et al.[23] found that water molecules form approximately three hydrogen bonds at the solid/liquid interface. Thus, the adsorption enthalpy of water can be calculated as the adsorption enthalpy of a single adsorbed water molecule plus the energetic contribution from three hydrogen bonds. The energy of a hydrogen bond was reported to be -7 kJ/mol.[20] Discussion on how to get enthalpy from DFT energy calculations is found in the Supporting Information. ΔH°_{vap} is the vaporization enthalpy for water (41 kJ/mol),[24] γ represents the surface energy of liquid water (0.073 J/m^2), while σ_A is the surface area of the adsorbate molecule A (0.56 nm^2 for 1/9 ML coverage on Rh(111)).[20,21,25] $\Delta H_{Solv,A}$ is the solvation enthalpy of species A in water, and were calculated using explicit solvation.

The enthalpies of adsorption were calculated following Akinola et al.[20] The adsorption enthalpies of gas-phase species were calculated using ideal-gas statistic mechanics. A summary of such an approach can be found in previous literature.[20,26,27] For gas phase molecules, the enthalpies were calculated with the following equation at 298.15 K, using DFT electronic energies (E). Zero point energies (E_{ZPE}) and the integral of the heat capacity with 298.15 K at constant pressure (1 atm) were also calculated. For a molecule in the gas-phase we have the following:

$$H(T) = E + E_{ZPE} + \int_0^T C_p dT. \tag{S7}$$

$$C_p = k_B + C_{v,trans} + C_{v,rot} + C_{v,vib} + C_{v,elec}. \tag{S8}$$

Here the first two terms of Equation S7 are the DFT electronic energy and the zero-point energy. The integral is over the constant-pressure heat capacity. The zero-point energies were calculated as $\sum \frac{1}{2} h\omega_i$, in which h is Planck's constant and ω_i is the vibrational frequency

calculated using finite differences. In Equation S8, the constant-pressure heat capacity is separable into translational, rotational, vibrational, and electronic parts, along with a k_B term for the conversion from constant-volume to constant-pressure. The translational heat capacity is 3/2 k_B for a 3-dimensional gas. The rotational heat capacity is 0 for a monatomic species, k_B for a linear molecule, and 3/2 k_B for a nonlinear molecule. The electronic component of the heat capacity is assumed to be 0. With regards to the vibrational heat capacity, there are 3N-6 degrees of freedom for nonlinear molecules and 3N-5 degrees of freedom for linear molecules (where N is the number of atoms). The vibrational contribution to the enthalpy is calculated from this integral:

$$\int_0^T C_{v,vib} dT = \sum_i^{vibDOF} \frac{\epsilon_i}{e^{\epsilon_i / k_B T} - 1}, \tag{S9}$$

where ϵ_i represents the energy due to the vibrational mode ω_i.

For the adsorbed species, enthalpies of adsorbed molecules were calculated with the harmonic limit approximation.[28] The internal energy and enthalpy are related by H(T) = U(T) + PV. A pressure of 1 atm was used in all cases. The PV term is typically small for solids at this pressure and is assumed to be negligible.[29–31] Therefore, enthalpies of adsorbed species were approximately equal to the calculated internal energies at finite temperature. For a strongly bound adsorbate, the rotational and translational degrees of freedom are lost,[27] and only vibrational energies are relevant for adsorbed species. We therefore ignored translational or rotational energy contributions. For the systems involving the surface, we used all calculated vibrational modes of the system, whether the bare surface, adsorbate+surface, solvent+surface, or adsorbate+solvent+surface. This gives the following for the enthalpy of adsorbed species A (or bare surface or surface with adsorbate and solvent).

$$H(T) \approx U(T) = E + E_{ZPE} + \sum_i^{vibrations} \frac{\epsilon_i}{e^{\epsilon_i / k_B T} - 1}. \tag{S10}$$

Therefore, the enthalpy of adsorption in vacuum at 298.15 K can be calculated as:

$$\Delta H^{\circ}_{ads,vac,A/surface} = H_{vac,A/surface} - H_{vac,A} - H_{vac,surface}. \tag{S11}$$

Here $H_{vac,A}$ is calculated with Equation S7, $H_{vac,A/surface}$ and $H_{vac,surface}$ are calculated with Equation S10.

5 Calculating Gibbs free energies

Gibbs free energies were calculated following previous literature.[20,26–28] Enthalpies and entropies were both calculated using ideal-gas statistical mechanics for gas phase molecules and the harmonic limit approximation for adsorbed species according to the following formula:

$$G(T,P) = H(T) - TS(T,P). \tag{S12}$$

Here, enthalpies $H(T)$ were calculated as discussed in Section 4, while entropies were calculated as discussed below

The entropies of gas-phase molecules were calculated as the following.

$$S(T,P) = S_{trans} + S_{rot} + S_{vib} + S_{elec} - k_B ln\frac{P}{P^o}. \tag{S13}$$

$$S_{trans} = k_B[ln[(\frac{2\pi M k_B T}{h^2})^{\frac{3}{2}}\frac{k_B T}{P^o}] + \frac{5}{2}]. \tag{S14}$$

Here, M is the molecule weight, and P^o is the standard pressure (1 atm).

$$S_{rot,linear} = R[ln(\frac{8\pi^2 I k_B T}{\sigma h^2}) + 1]. \tag{S15}$$

$$S_{rot,non-linear} = R[ln[(\frac{\sqrt{\pi I_A I_B I_C}}{\sigma})(\frac{8\pi^2 k_B T}{h^2})^{3/2}] + \frac{3}{2}]. \tag{S16}$$

I_i are the moments of inertia of the molecules, and σ is the symmetry number.

$$S_{vib} = k_B \sum_{i}^{vibDOF} [\frac{\epsilon_i}{k_B T(e^{\epsilon_i/k_B T} - 1)} - ln(1 - e^{-\epsilon_i/k_B T})]. \tag{S17}$$

$$S_{elec} = k_B ln[2 \times (total\ spin) + 1]. \tag{S18}$$

where *total spin* is the spin multiplicity of molecules. ($\frac{1}{2}$ for doublet, 1 for triplet, etc.)

For a strongly bound adsorbate, the rotational and translational entropic contributions are less relevant,[27] and vibrations are the dominant contributor to entropy. Entropies of adsorbed molecules were calculated with the harmonic approximation according to following formula:[26,32]

$$S(T, P) = k_B \sum_{i}^{vibrations} [\frac{\epsilon_i}{k_B T(e^{\epsilon_i/k_B T} - 1)} - ln(1 - e^{-\epsilon_i/k_B T})]. \tag{S19}$$

Similar to the enthalpy calculations, we used all calculated vibrational modes for calculating entropies of the surface, adsorbate+surface, solvent+surface, and adsorbate+solvent+surface systems.

6 Validation of Bond-Additivity Results

We sought to validate our approach to calculating explicit solvation enthalpies by comparing solvation enthalpies of free species (not adsorbed) to experimental data. We used the implicit, explicit and hybrid methods to calculate the solvation enthalpies of free species in water. When using the implicit method, the species were modeled with VASPsol and a dielectric constant of 78.4. The solvation enthalpy $\Delta H_{Solv,A}$ of molecule A was calculated using the

following:

$$\Delta H_{Solv,A} = H^{sol}_{A(gas)} - H^{vac}_{A(gas)}. \tag{S20}$$

When using the explicit method, solvation enthalpy $\Delta H_{Solv,A}$ was calculated as:

$$\Delta H_{Solv,A} = H_{A+H_2O(gas)} - H_{A(gas)} - H_{H_2O(gas)}. \tag{S21}$$

The enthalpies of the gas phase molecules were calculated with the ideal-gas assumptions discussed in the previous section. In this equation, $\Delta H_{Solv,A}$ is the solvation enthalpy for species A in water. $H_{A-H_2O,gas}$ is the enthalpy of a molecule A/water complex. $H_{A(gas)}$ and $H_{H_2O(gas)}$ are the enthalpies for molecules A and H_2O in the gas phase. As for hybrid models, explicit water molecules were added to the simulation while implicit solvation was also applied. Optimized explicit solvent configurations were chsoen as the starting point and then applied implicit solvation for these hybrid calculations. Solvation enthalpies of 17 different molecules in water were calculated to validate our approach. The results were compared with solvation energies obtained by applying the van't Hoff equation using Henry's law constants from Sander's work:[33]

$$\frac{dlnK_H}{d(\frac{1}{T})} = \frac{-\Delta H_{solv}}{R}. \tag{S22}$$

Table S5 shows our calculated solvation energies compared to experimentally-derived solvation enthalpies. Table S6 also provides solvation enthalpies, $\Delta H_{Solv,A}$, of species relevant to C-C and C-H reactions we studied. Compared to experimentally-derived solvation enthalpies, the calculated solvation enthalpies using the implicit method were 0.21 eV larger on average, and the average calculated solvation enthalpies using the explicit and hybrid methods were 0.05 and 0.09 eV larger than the experimental-derived solvation enthalpies, respectively. Thus, using the explicit method to predict select species' adsorption enthalpies

showed more consistent results to the experimental values than using implicit and hybrid methods, and we chose to use the explicit method for the solvation enthalpies of species in our ethanol C-C and C-H bond cleavage reactions. Table S5 also shows that using the explicit method, for smaller molecules (like O_2, CO, CO_2, etc.), our results match very well with the experimental results, and the enthalpy differences are within 0.1 eV. For larger molecules, like ethanol or methanol, the enthalpy differences may be slightly larger (0.1 to 0.2 eV), but our results still match reasonably well with experiment. The average difference between our calculated solvation energies and the experimentally-derived solvation energies was 0.05 eV, and the maximum energy difference was 0.2 eV. Overall, the agreement between theory (explicit solvation) and experiment is quite good.

Table S5: Comparison of calculated solvation enthalpies for free species compared to experimental solvation enthalpies. Values are in eV.

	Implicit	Explicit	Hybrid	van't Hoff equation
N_2	0.02	-0.08	-0.11	-0.11
NO	0.03	-0.12	-0.13	-0.14
NO_2	-0.02	-0.15	-0.12	-0.21
NH_3	-0.19	-0.40	-0.34	-0.32
O_2	0.11	-0.12	-0.11	-0.13
CO	-0.01	-0.12	-0.11	-0.12
CO_2	-0.07	-0.14	-0.12	-0.21
CH_4	0.02	-0.12	-0.10	-0.15
C_2H_2	-0.13	-0.22	-0.16	-0.16
HCl	-0.12	-0.33	-0.41	-0.19
H_2O_2	-0.28	-0.40	-0.39	-0.60
CH_3OH	-0.19	-0.31	-0.25	-0.47
CH_3CH_2OH	-0.19	-0.34	-0.23	-0.53
HCOOH	-0.31	-0.46	-0.37	-0.51
CH_3COOH	-0.29	-0.44	-0.35	-0.54
Phenol	-0.23	-0.38	-0.33	-0.51
Cyclohexanol	-0.15	-0.56	-0.45	-0.67

Table S6: Calculated solvation enthalpies for ethanol component species involved in C-C and C-H scission using explicit solvation.

	$\Delta H_{Solv,A}$ (eV)
CH_3CH_2OH	-0.34
CH_3CH_2O	-0.37
CH_2CH_2O	-0.26
CH_2OH	-0.60
CH_2O	-0.23
CH_3CO	-0.27
CH_2CO	-0.19
CHCO	-0.28
CH_3	-0.13
CH_2	-0.32
CH	-0.92
CO	-0.12
H	-0.11

We also compared our bond-additivity enthalpies with literature values. Our enthalpy changes upon applying the bond-additivity method are consistent with previous work. In Akinola et al.'s work,[20] they calculated adsorption enthalpies for organics (benzaldehyde, benzyl alcohol, cyclohexanol, furfural, and phenol) on the (111), (110), and (100) surfaces of Pt and Rh. They predicted adsorption enthalpies using the bond-additivity model in the aqueous phase to be more endothermic than gas phase results by an average value of 2.07 eV, with the smallest and largest enthalpy increases being 0.81 and 3.44 eV. Comparing implicit solvation and bond-additivity methods, their adsorption enthalpies also increased using the bond-additivity method by 2.24 eV on average, and the smallest and largest enthalpy changes were 1.07 and 3.51 eV, respectively. They showed that using implicit solvation model could lead to far more exothermic adsorption enthalpies than experimental adsorption measurements, while the bond-additivity model gave results closer to experiment. In our case, using the bond-additivity method also led to far more endothermic values for adsorption enthalpies compared to vacuum and implicit solvation, in agreement with Akinola et al.'s work. Furthermore, We calculated the bond-additivity adsorption enthalpy for adsorbed CO over Rh(111) to be -1.17 eV. He et al. reported the heat of adsorption of CO to range from

around -1.65 to 0.21 eV over Rh catalysts.[34] The adsorption energy of CO on Rh(111) was reported to range from around -1.65 to -0.6 eV, as a function of CO coverage.[35] At lower CO coverage the CO adsorption energy was reported to range from -1.39 to -0.78 eV also over Rh(111).[36] Our calculated value is consistent with these range of experimental values reported in the literature, again validating our results using the bond-additivity method.

7 Optimized Geometries in Water Solvent

Geometries of the various adsorbed species, both in a vacuum and using different solvent models, are given in Figures S10 to S24. The optimized structures of the reaction intermediates in implicit water solvent are very close to vacuum structures. In Tables S7 to S21, the bond lengths within adsorbates and between the adsorbates and metal surfaces are given. As indicated, the bond lengths within adsorbate molecules only changed by up to 0.01 Å for all the adsorbed species when using implicit water solvation compared to vacuum. The maximum and minimum bond length changes when using implicit solvation were 0.01 and 0.00 Å, respectively, with an average change of 0.00 Å. Moreover, the largest change with implicit solvation in the distance between the adsorbate and metal surface was 0.08 Å while the smallest distance change was 0.00 Å. The average change in distance between adsorbate molecules and the surface was 0.01 Å.

The most stable geometries with explicit solvation have the hydrogen atoms of the water solvent molecules interacting with O atoms of the adsorbates, forming a hydrogen bond. When using the explicit solvation model, the maximum and minimum bond length changes (compared to vacuum) within the adsorbed species were 0.03 and 0.00 Å, respectively, and the average bond distance change was only 0.01 Å with a standard deviation of 0.01 Å. As for the distances between adsorbates and the metal surface, the distances changed only with an average value of 0.03Å, while the minimal and maximum surface-adsorbate distances changes were 0.00 and 0.18 Å. When using the explicit+ model, the bond length changes

within the adsorbates were in the range of 0.00 to 0.05 Å. The average length change was 0.01 Å with a standard deviation of 0.01 Å. The largest change in distance between the adsorbates and surfaces with explicit solvation was 0.17 Å, while the smallest change was 0 Å. The average distance change was 0.03 Å with a standard deviation of 0.04 Å. Thus, the adsorbates' structures were not affected considerably by explicit water molecules, while the distances between the adsorbates and metal surfaces were affected only slightly more.

Upon hydrogen bond formation, with explicit water solvation models, the water molecules interacted weakly with the CH_3CH_2OH, CH_3CH_2O, CH_2O, CH_2, and CH_3COOH adsorbates with an average H-bond distance of 2.57 Å. Stronger H-bonds formed for species CH_2CH_2O, CH_2OH, CH_3CO, CH_2CO, CHCO, CO, and OH with an average hydrogen bond distance of 1.73 Å. However, the water molecules did not interact with the CH_3, CH, and H species, and the distances between these adsorbates and the water molecules was greater than 3 Å.

When using the explicit+ models, both of the two water molecules were bound to the adsorbates for some species: CH_2CH_2O, CH_2OH, CH_2O, CH_2CO, and CO. For CH_3CH_2OH, CH_3CO, CHCO, CH_2, CH_3COOH and OH species, only one water molecule bound to the adsorbate, while the other water molecule bound to the first water molecule. We optimized structures for ethanol, CH_3CO, CHCO, CH_2, CH_3COOH and OH where two water molecules interacted with the adsorbates, but they converged to the structures with only one water molecule interacting with the adsorbate. However, for CH_3CH_2O, CH_3, CH and H species, neither of the two water molecules interacted with the adsorbates. The distances between water and adsorbate were beyond 3 Å in these cases. The average hydrogen bond distance between the water and all adsorbates was 1.83 Å, while the average length of the hydrogen bonds between the water molecules was 1.69 Å.

When applying the hybrid model, the largest bond length change of the adsorbed species was 0.03 Å, while the smallest change was 0.00 Å. The average bond length change was 0.01 Å with a standard deviation of 0.01 Å. The distance change between the adsorbates and metal surfaces was in a range of 0.00 to 0.18 Å with an average value of 0.02 Å. Thus, like the explicit

and explicit+ models, the hybrid approach had minimal effect on adsorbates' structures, while the distance between the adsorbates and metal surfaces was affected slightly more. As for hydrogen bonding, the water molecules interacted strongly with species like CH_2CH_2O, CH_2OH, CH_3CO, CH_2CO, CHCO and OH with an average hydrogen bond distance of 1.71 Å. On the other hand weaker hydrogen bonds were formed with ethanol, CH_3CH_2O, CH_2O, CH_2, CO and CH_3COOH species with an average length of 2.57 Å. However, for CH_3, CH, and H, the distances between the solvent molecules and adsorbates were beyond 3 Å.

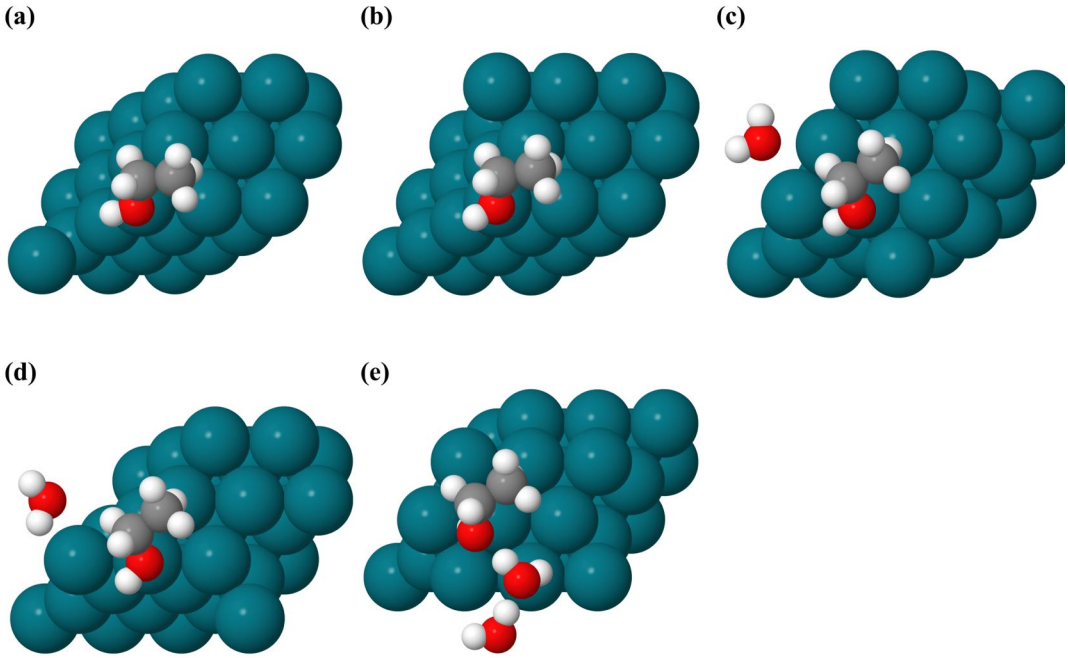

Figure S10: Optimized ethanol structures adsorbed on Rh(111) in (a)vacuum. Also given are structures using (b)implicit, (c)explicit, (d)hybrid, and (e)explicit+ water solvation approaches.

Table S7: Bond lengths of optimized ethanol adsorbed on Rh(111) in various water solvation environments.

Bond Length (Å)					
	vacuum	implicit	explicit	hybrid	explicit+
C_1-O	1.46	1.47	1.46	1.46	1.45
C_1-C_2	1.51	1.51	1.51	1.51	1.52
C-H	1.10	1.10	1.10	1.10	1.10
O-H	0.98	0.98	0.99	0.98	0.99
O-Rh	2.31	2.23	2.42	2.3	-
H bond(water-ads)	-	-	2.86	2.75	1.7
H bond(water-water)	-	-	-	-	1.59

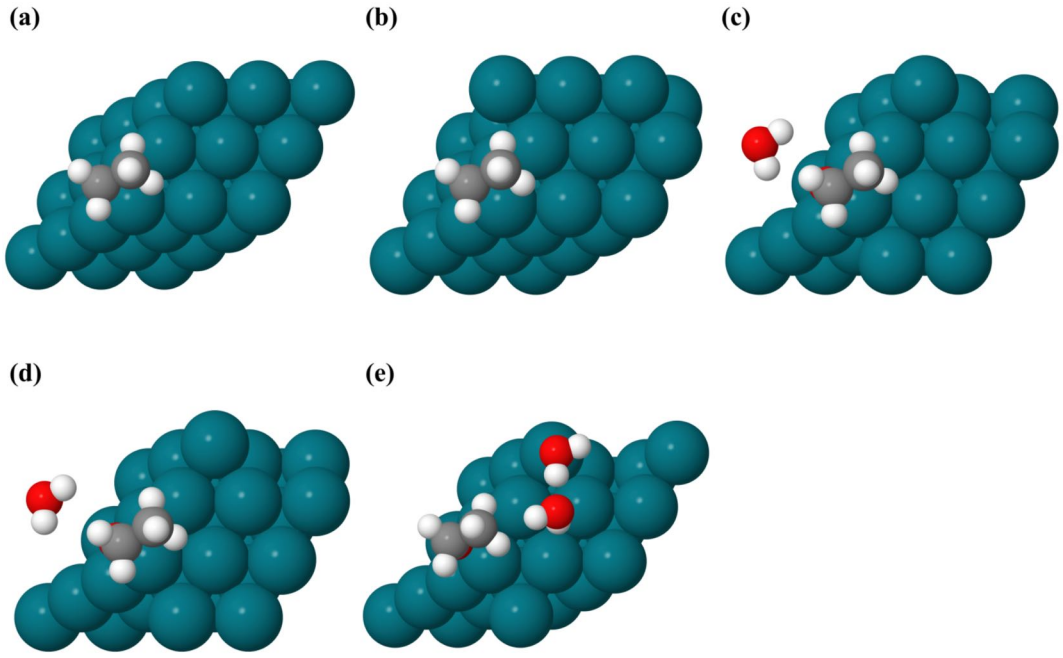

Figure S11: Optimized CH_3CH_2O structures adsorbed on Rh(111) in (a)vacuum. Also given are structures using (b)implicit, (c)explicit, (d)hybrid, and (e)explicit+ water solvation approaches.

Table S8: Bond lengths of optimized structures of CH_3CH_2O adsorbed on Rh(111) in various water solvation environments.

Bond Length (Å)					
	vacuum	implicit	explicit	hybrid	explicit+
C_1-O	1.44	1.45	1.44	1.45	1.44
C_1-C_2	1.51	1.51	1.52	1.51	1.52
C-H	1.10	1.10	1.10	1.10	1.10
O-Rh	2.17	2.16	2.16	2.14	2.24
H bond(water-ads)	-	-	2.73	2.87	-
H bond(water-water)	-	-	-	-	1.68

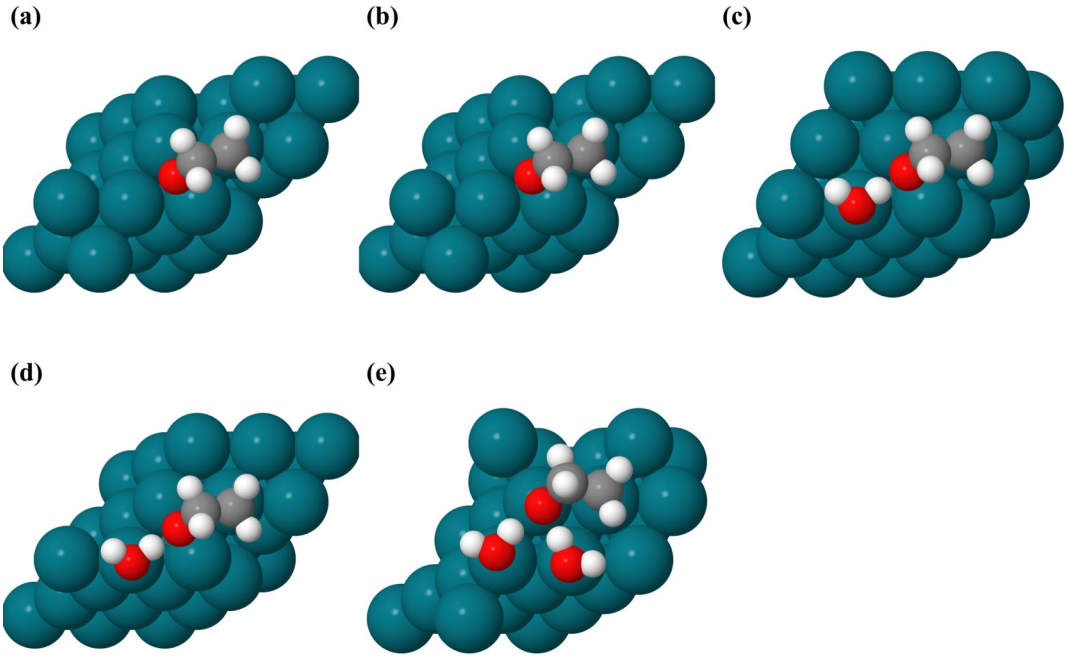

Figure S12: Optimized CH_2CH_2O structures adsorbed on Rh(111) in (a)vacuum. Also given are structures using (b)implicit, (c)explicit, (d)hybrid, and (e)explicit+ water solvation approaches.

Table S9: Bond lengths of optimized structures of CH_2CH_2O adsorbed on Rh(111) in various water solvation environments.

	Bond Length (Å)				
	vacuum	implicit	explicit	hybrid	explicit+
C_1-O	1.45	1.45	1.45	1.45	1.43
C_1-C_2	1.52	1.52	1.51	1.51	1.52
C-H	1.10	1.10	1.10	1.10	1.10
O-Rh_1	2.13	2.13	2.28	2.24	-
O-Rh_2	2.11	2.11	2.16	2.14	2.11
C_2-Rh	2.11	2.10	2.10	2.10	2.11
H bond(water-ads)	-	-	1.48	1.51	1.52;1.70

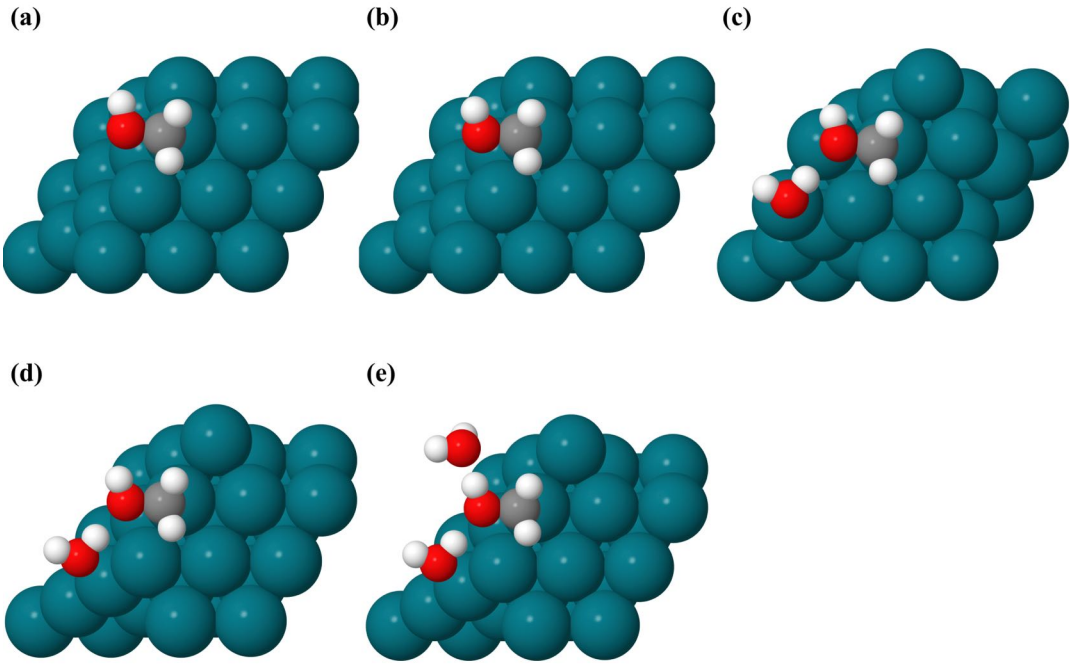

Figure S13: Optimized CH_2OH structures adsorbed on Rh(111) in (a)vacuum. Also given are structures using (b)implicit, (c)explicit, (d)hybrid, and (e)explicit+ water solvation approaches.

Table S10: Bond lengths of optimized structures of CH_2OH adsorbed on Rh(111) in various water solvation environments.

Bond Length (Å)					
	vacuum	implicit	explicit	hybrid	explicit+
C-O	1.46	1.45	1.47	1.47	1.46
C-H	1.10	1.10	1.10	1.10	1.10
C-Rh	2.07	2.07	2.06	2.06	2.07
O-H	0.99	0.98	0.99	0.98	1.02
H bond(water-ads)	-	-	1.95	1.85	1.84;1.65

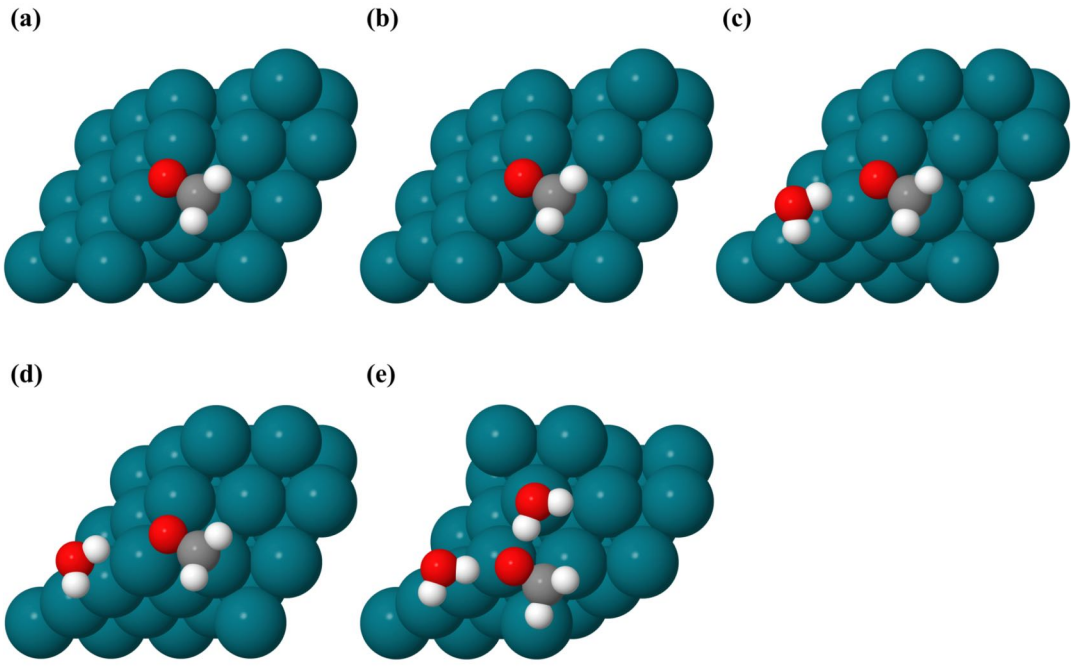

Figure S14: Optimized CH_2O structures adsorbed on Rh(111) in (a)vacuum. Also given are structures using (b)implicit, (c)explicit, (d)hybrid, and (e)explicit+ water solvation approaches.

Table S11: Bond lengths of optimized structures of CH_2O adsorbed on Rh(111) in various water solvation environments.

Bond Length (Å)					
	vacuum	implicit	explicit	hybrid	explicit+
C-O	1.38	1.39	1.39	1.39	1.38
C-H	1.10	1.10	1.10	1.10	1.11
O-Rh_1	2.17	2.17	2.17	2.18	2.13
O-Rh_2	2.17	2.17	2.23	2.18	-
C-Rh	2.08	2.08	2.08	2.08	2.17
H bond(water-ads)	-	-	2.51	2.99	1.91;1.62

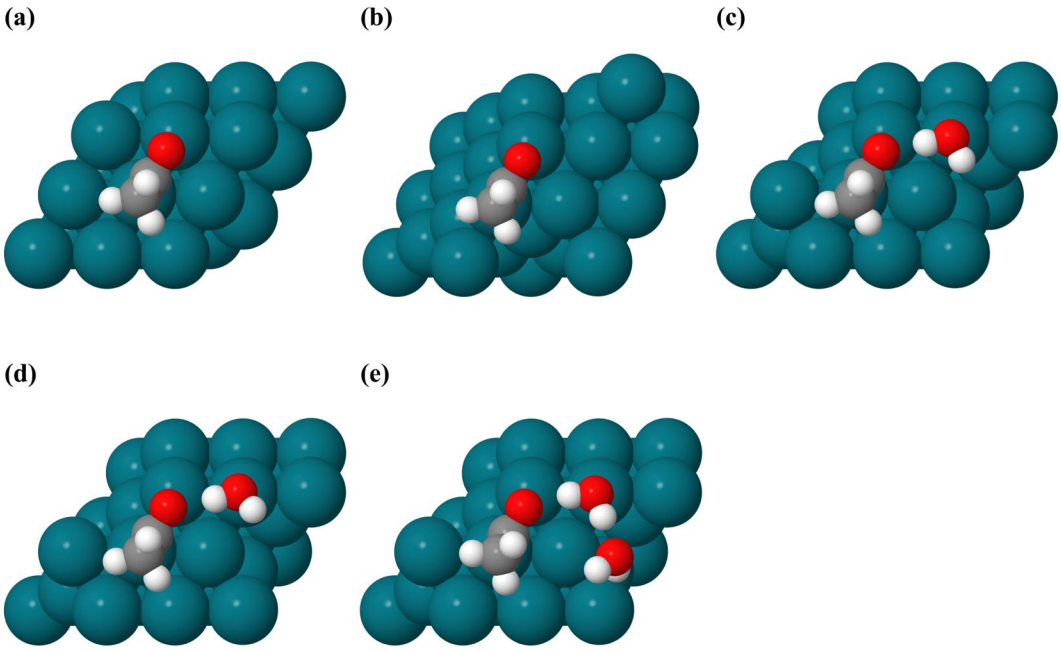

Figure S15: Optimized CH_3CO structures adsorbed on Rh(111) in (a)vacuum. Also given are structures using (b)implicit, (c)explicit, (d)hybrid, and (e)explicit+ water solvation approaches.

Table S12: Bond lengths of optimized structures of CH_3CO adsorbed on Rh(111) in various water solvation environments.

Bond Length (Å)					
	vacuum	implicit	explicit	hybrid	explicit+
C_1-O	1.26	1.27	1.28	1.28	1.28
C_1-C_2	1.50	1.50	1.51	1.50	1.50
C-H	1.10	1.10	1.10	1.10	1.10
O-Rh	2.16	2.15	2.20	2.18	2.19
C_1-Rh	1.96	1.96	1.94	1.95	1.95
H bond(water-ads)	-	-	1.88	1.95	1.94
H bond(water-water)	-	-	-	-	1.76

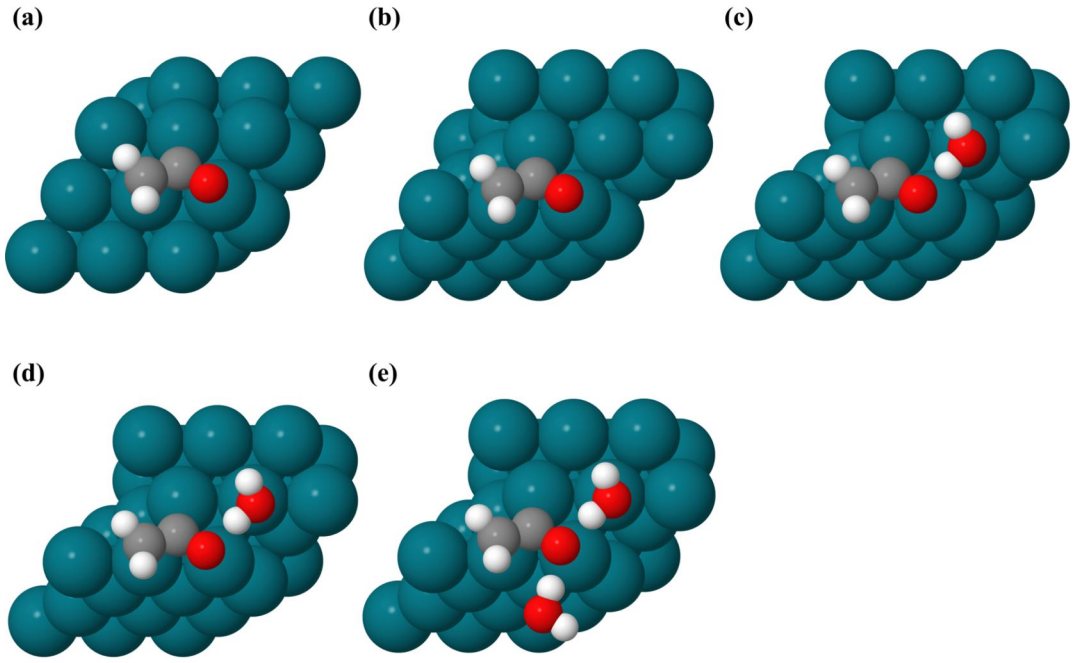

Figure S16: Optimized CH_2CO structures adsorbed on Rh(111) in (a)vacuum. Also given are structures using (b)implicit, (c)explicit, (d)hybrid, and (e)explicit+ water solvation approaches.

Table S13: Bond lengths of optimized structures of CH_2CO adsorbed on Rh(111) in various water solvation environments.

Bond Length (Å)					
	vacuum	implicit	explicit	hybrid	explicit+
C_1-O	1.29	1.29	1.32	1.31	1.34
C_1-C_2	1.44	1.44	1.43	1.43	1.43
C-H	1.10	1.10	1.10	1.10	1.10
O-Rh	2.11	2.12	2.16	2.15	2.21
C_1-Rh_1	2.49	2.49	2.53	2.52	2.57
C_1-Rh_2	2.28	2.28	2.23	2.23	2.22
C_1-Rh_3	2.05	2.05	2.05	2.05	2.04
C_2-Rh	2.17	2.17	2.18	2.17	2.18
H bond(water-ads)	-	-	1.66	1.72	1.72;1.74

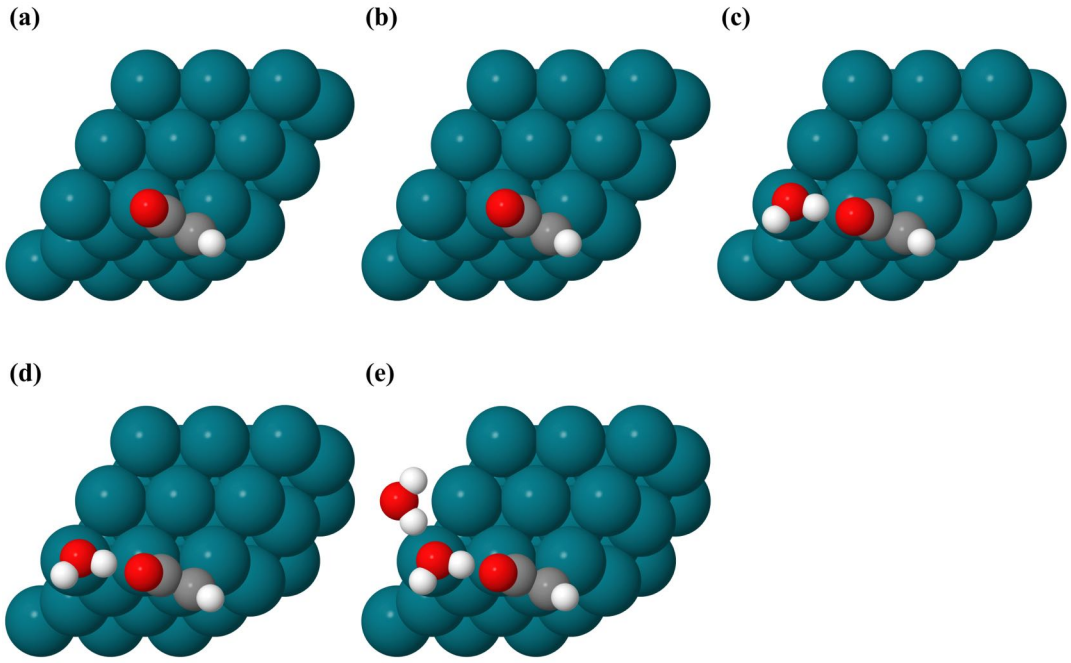

Figure S17: Optimized CHCO structures adsorbed on Rh(111) in (a)vacuum. Also given are structures using (b)implicit, (c)explicit, (d)hybrid, and (e)explicit+ water solvation approaches.

Table S14: Bond lengths of optimized structures of CHCO adsorbed on Rh(111) in various water solvation environments.

Bond Length (Å)					
	vacuum	implicit	explicit	hybrid	explicit+
C_1-O	1.21	1.21	1.24	1.24	1.25
C_1-C_2	1.44	1.44	1.44	1.44	1.44
C-H	1.10	1.10	1.10	1.10	1.10
C_1-Rh	2.05	2.05	2.01	2.01	2.00
C_2-Rh	2.06	2.06	2.06	2.05	2.06
H bond(water-ads)	-	-	1.62	1.66	1.52
H bond(water-water)	-	-	-	-	1.75

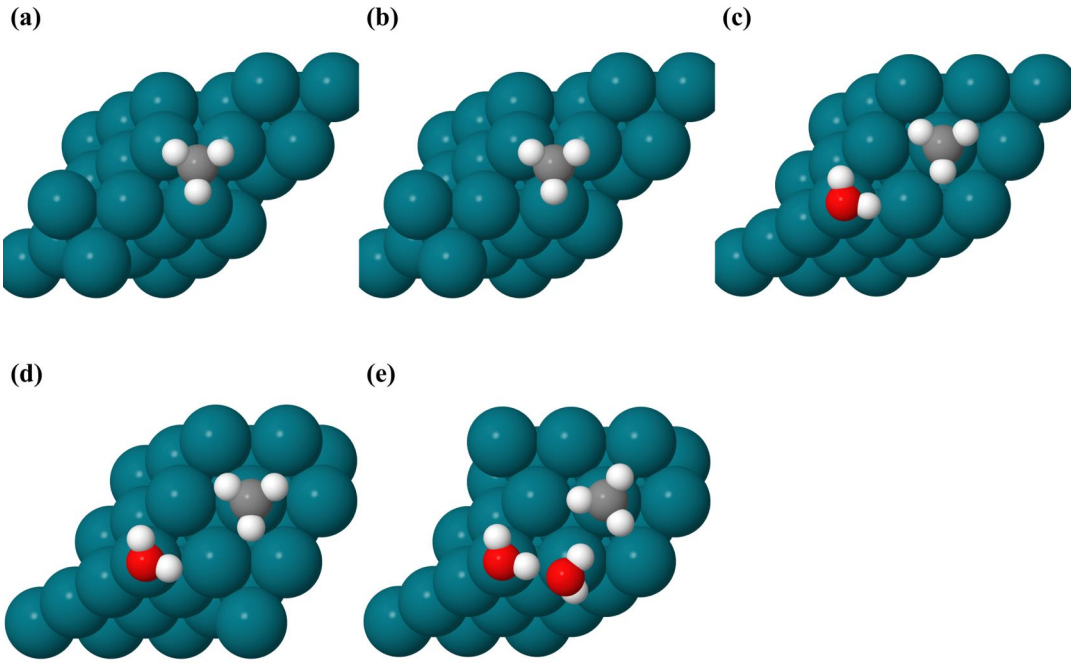

Figure S18: Optimized CH_3 structures adsorbed on Rh(111) in (a)vacuum. Also given are structures using (b)implicit, (c)explicit, (d)hybrid, and (e)explicit+ water solvation approaches.

Table S15: Bond lengths of optimized structures of CH_3 adsorbed on Rh(111) in various water solvation environments.

Bond Length (Å)					
	vacuum	implicit	explicit	hybrid	explicit+
C-H	1.12	1.13	1.10	1.10	1.10
C-Rh_1	2.26	2.25	2.08	2.08	2.09
C-Rh_2	2.26	2.25	-	-	-
C-Rh_3	2.27	2.25	-	-	-
H bond(water-water)	-	-	-	-	1.68

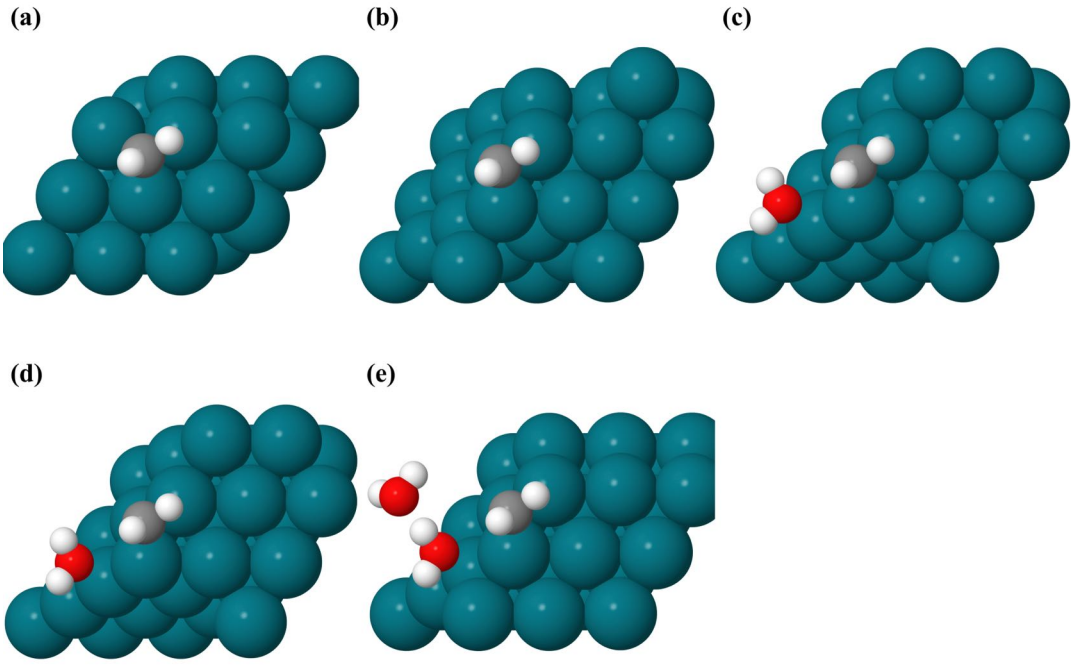

Figure S19: Optimized CH_2 structures adsorbed on Rh(111) in (a)vacuum. Also given are structures using (b)implicit, (c)explicit, (d)hybrid, and (e)explicit+ water solvation approaches.

Table S16: Bond lengths of optimized structures of CH_2 adsorbed on Rh(111) in various water solvation environments.

Bond Length (Å)					
	vacuum	implicit	explicit	hybrid	explicit+
C-H	1.10	1.10	1.10	1.10	1.10
C-Rh_1	2.03	2.03	2.04	2.04	2.04
C-Rh_2	2.03	2.03	2.04	2.04	2.04
C-Rh_3	2.16	2.15	2.16	2.15	2.15
H bond(water-ads)	-	-	2.66	2.59	2.58
H bond(water-water)	-	-	-	-	1.70

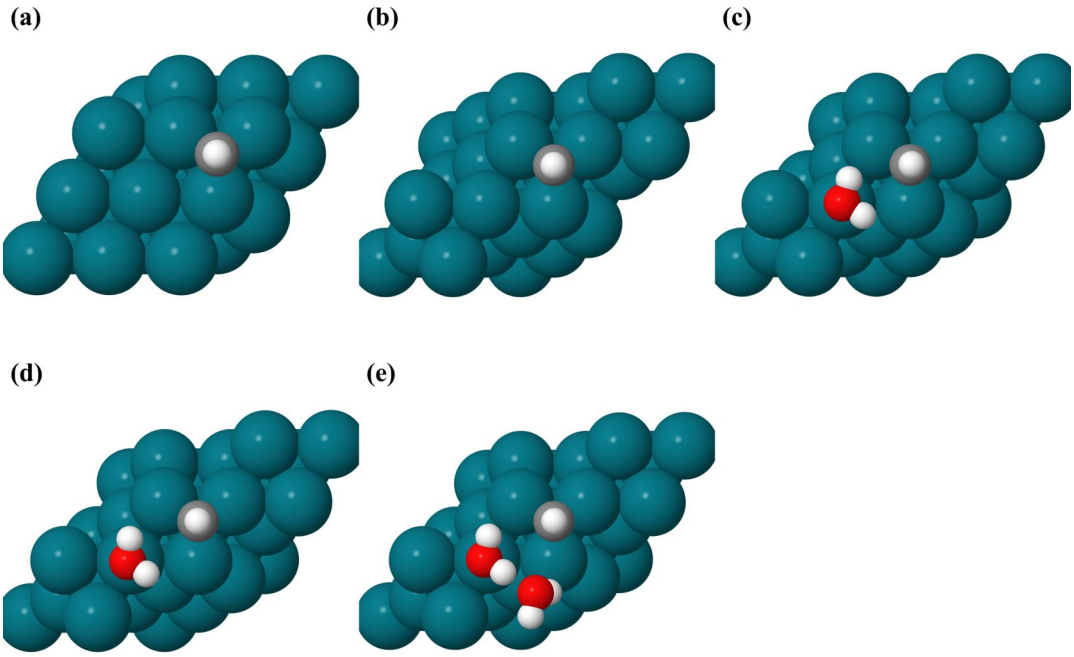

Figure S20: Optimized CH structures adsorbed on Rh(111) in (a)vacuum. Also given are structures using (b)implicit, (c)explicit, (d)hybrid, and (e)explicit+ water solvation approaches.

Table S17: Bond lengths of optimized structures of CH adsorbed on Rh(111) in various water solvation environments.

Bond Length (Å)					
	vacuum	implicit	explicit	hybrid	explicit+
C-H	1.10	1.10	1.10	1.10	1.10
C-Rh_1	1.98	1.98	1.99	1.99	1.99
C-Rh_2	1.98	1.98	1.99	1.99	1.99
C-Rh_3	1.98	1.98	1.98	1.98	1.98
H bond(water-water)	-	-	-	-	1.68

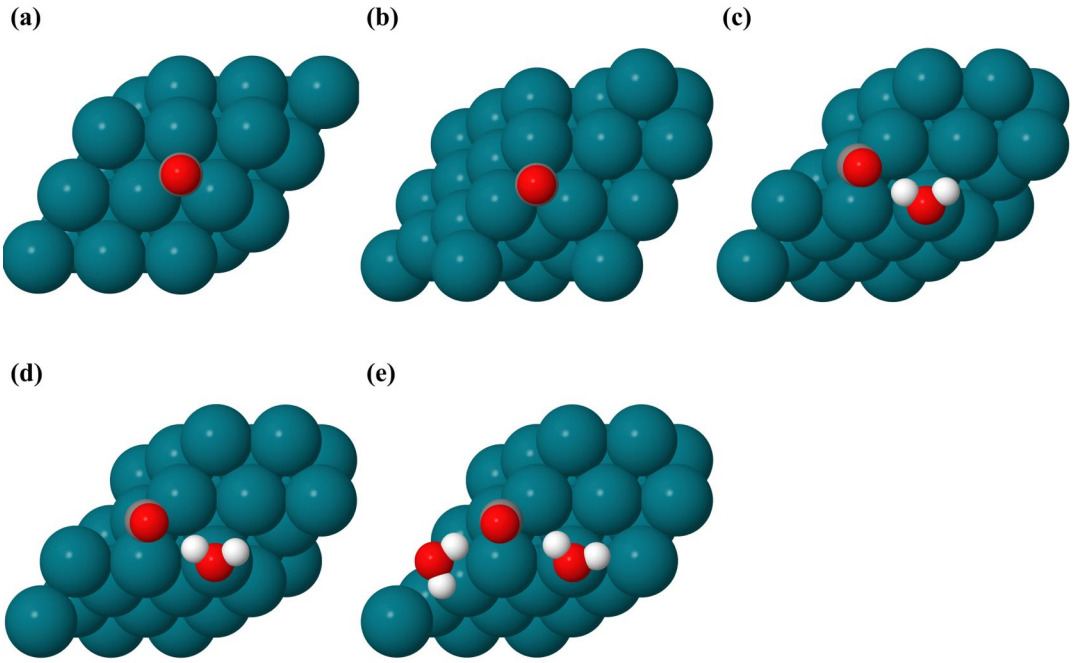

Figure S21: Optimized CO structures adsorbed on Rh(111) in (a)vacuum. Also given are structures using (b)implicit, (c)explicit, (d)hybrid, and (e)explicit+ water solvation approaches.

Table S18: Bond lengths of optimized structures of CO adsorbed on Rh(111) in various water solvation environments.

Bond Length (Å)					
	vacuum	implicit	explicit	hybrid	explicit+
C-O	1.20	1.20	1.22	1.22	1.23
C-Rh_1	2.10	2.10	2.08	2.08	2.08
C-Rh_2	2.10	2.10	2.08	2.08	2.08
C-Rh_3	2.10	2.10	2.08	2.08	2.05
H bond(water-ads)	-	-	1.91	2.05	2.35;1.97

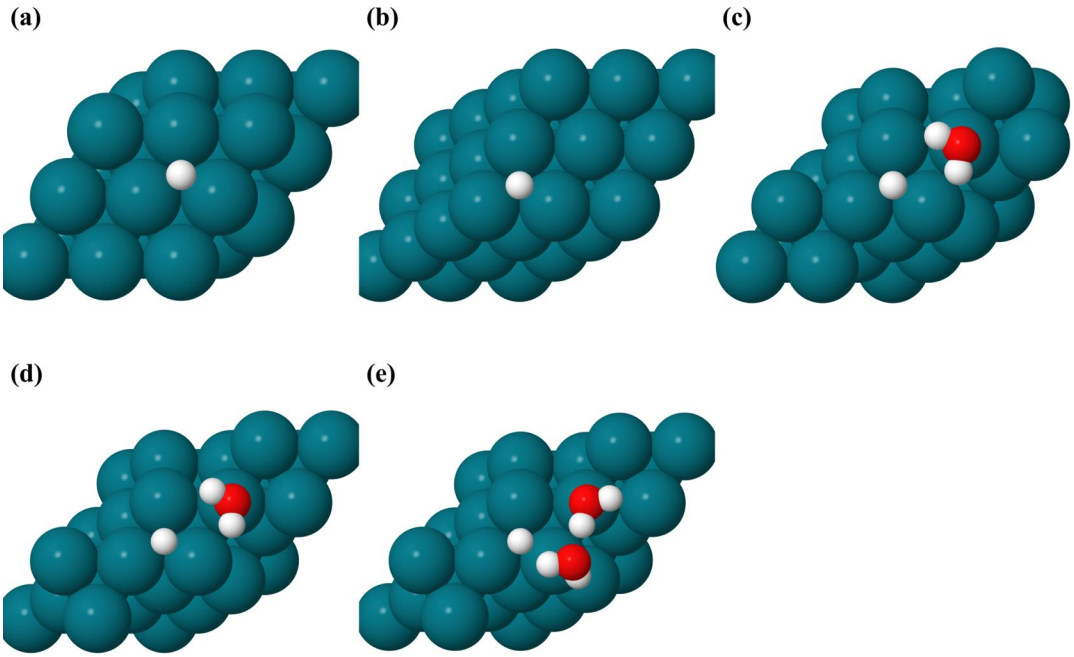

Figure S22: Optimized H structures adsorbed on Rh(111) in (a)vacuum. Also given are structures using (b)implicit, (c)explicit, (d)hybrid, and (e)explicit+ water solvation approaches.

Table S19: Bond lengths of optimized structures of H adsorbed on Rh(111) in various water solvation environments.

Bond Length (Å)					
	vacuum	implicit	explicit	hybrid	explicit+
H-Rh_1	1.86	1.86	1.86	1.86	1.85
H-Rh_2	1.86	1.86	1.86	1.85	1.87
H-Rh_3	1.86	1.86	1.87	1.86	1.85
H bond(water-water)	-	-	-	-	1.68

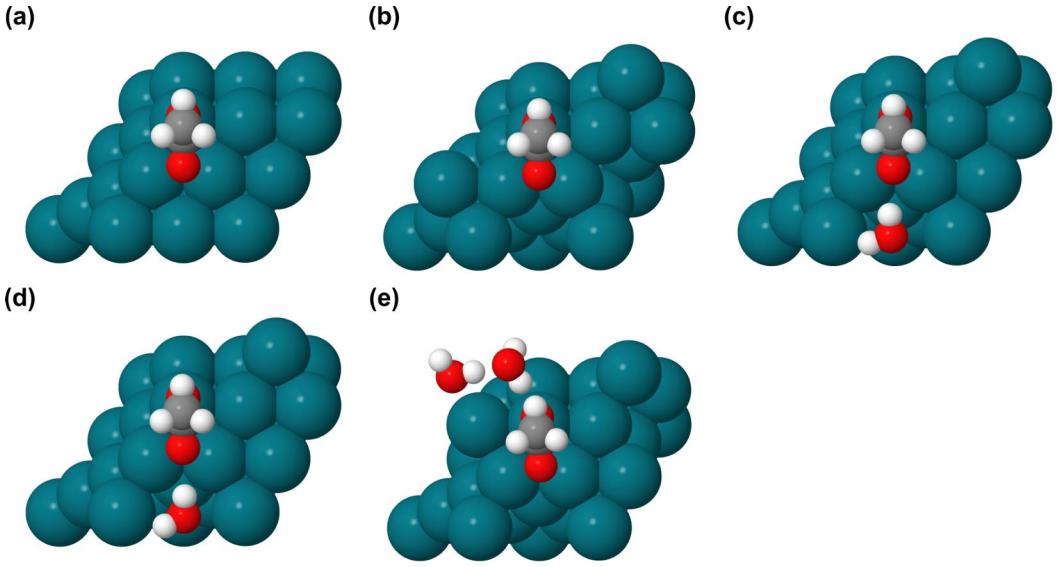

Figure S23: Optimized CH_3COOH structures adsorbed on Rh(111) in (a)vacuum. Also given are structures using (b)implicit, (c)explicit, (d)hybrid, and (e)explicit+ water solvation approaches.

Table S20: Bond lengths of optimized structures of CH_3COOH adsorbed on Rh(111) in various water solvation environments.

Bond Length (Å)					
	vacuum	implicit	explicit	hybrid	explicit+
C_1-O_1	1.25	1.25	1.24	1.25	1.25
C_1-O_2	1.32	1.32	1.33	1.33	1.32
O_2-H	1.02	1.02	1.04	1.04	1.04
C-H	1.10	1.09	1.09	1.09	1.10
C_1-C_2	1.50	1.49	1.50	1.49	1.50
O_1-Rh	2.17	2.15	2.22	2.18	2.29
H bond(water-ads)	-	-	2.1	2.14	1.84
H bond(water-water)	-	-	-	-	1.69

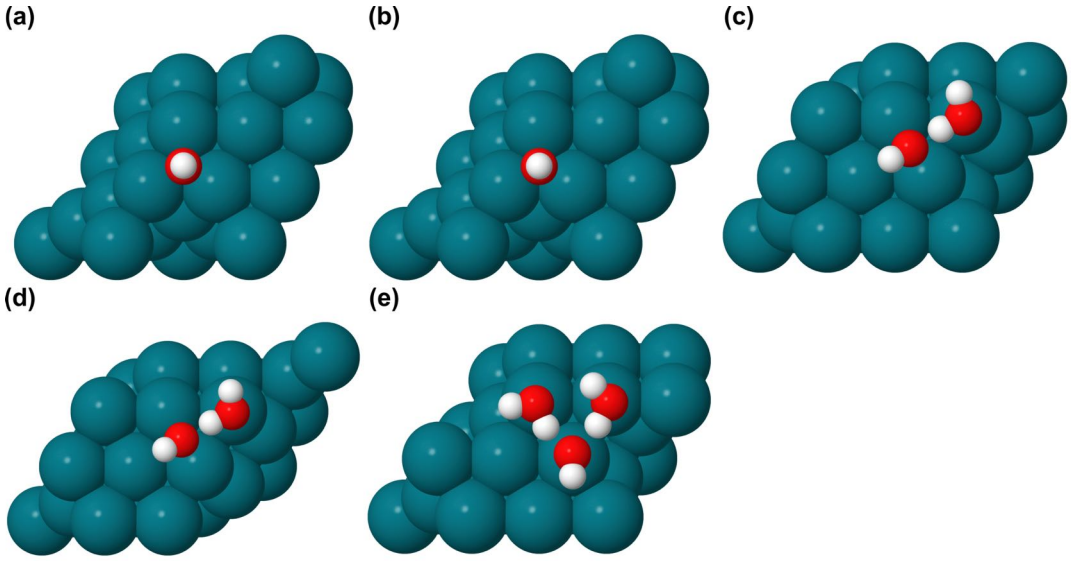

Figure S24: Optimized OH structures adsorbed on Rh(111) in (a)vacuum. Also given are structures using (b)implicit, (c)explicit, (d)hybrid, and (e)explicit+ water solvation approaches.

Table S21: Bond lengths of optimized structures of OH adsorbed on Rh(111) in various water solvation environments.

Bond Length (Å)					
	vacuum	implicit	explicit	hybrid	explicit+
O-H_1	0.97	0.98	0.98	0.98	0.98
O-Rh_1	2.16	2.14	2.19	2.17	2.12
O-Rh_2	2.17	2.14	2.19	2.17	-
O-Rh_3	2.17	2.14	-	-	-
H bond(water-ads)	-	-	1.60	1.59	1.54;1.58

8 Summary of Water Solvation Energies

All the adsorption and reaction free energies for the various water solvation results are given in Tables S22 and S23.

Table S22: Adsorption free energies on Rh(111) in water solvent of species relevant to ethanol oxidation. Results are shown in vacuum and with various solvation models.

ΔG_{ads} (eV)					
	vacuum	implicit	explicit	hybrid	explicit+
$*CH_3CH_2OH$	0.12	0.12	0.20	0.31	-0.01
$*CH_3CH_2O$	-1.61	-1.53	-1.47	-1.37	-1.41
$*CH_2CH_2O$	-0.67	-0.60	-0.80	-0.53	-0.57
$*CH_2OH$	-1.44	-1.45	-1.45	-1.30	-1.46
$*CH_2O$	-0.29	-0.17	-0.30	-0.09	-0.30
$*CH_3CO$	-1.79	-1.74	-1.83	-1.64	-1.72
$*CH_2CO$	-0.79	-0.76	-0.92	-0.71	-0.86
$*CHCO$	-2.91	-2.84	-3.18	-2.90	-3.15
$*CH_3$	-1.33	-1.38	-1.29	-1.27	-1.20
$*CH_2$	-3.60	-3.62	-3.58	-3.55	-3.51
$*CH$	-6.17	-6.12	-6.12	-6.05	-6.08
$*CO$	-1.45	-1.52	-1.57	-1.49	-1.54
$*H$	-0.39	-0.39	-0.40	-0.39	-0.35
$*CH_3COOH$	-0.03	0.10	0.04	0.31	0.02
$*OH$	-2.57	-2.56	-2.74	-2.48	-2.78

Table S23: Reaction free energies on Rh(111) in water solvent of species relevant to ethanol oxidation. Results are shown in vacuum and with various solvation models.

ΔG_{rxn} (eV)					
	vacuum	implicit	explicit	hybrid	explicit+
$*CH_3CH_2OH + * \rightarrow *CH_3 + *CH_2OH$	0.38	0.30	0.33	0.36	0.61
$*CH_3CH_2O + * \rightarrow *CH_3 + *CH_2O$	0.28	0.24	0.18	0.28	0.20
$*CH_2CH_2O + * \rightarrow *CH_2 + *CH_2O$	-0.13	-0.18	0.01	-0.09	-0.15
$*CH_3CO + * \rightarrow *CH_3 + *CO$	-0.43	-0.49	-0.47	-0.45	-0.47
$*CH_2CO + * \rightarrow *CH_2 + *CO$	-0.80	-0.86	-0.78	-0.81	-0.74
$*CHCO + * \rightarrow *CH + *CO$	-1.06	-1.05	-0.88	-0.90	-0.82
$*CH_3CO + * \rightarrow *CH_2CO + *H$	0.10	0.11	0.00	0.06	0.00
$*CH_2CO + * \rightarrow *CHCO + *H$	-0.35	-0.39	-0.50	-0.50	-0.48
$*CH_3CO + *OH \rightarrow *CH_3COOH + *$	-0.13	-0.06	0.13	-0.04	0.06

9 Optimized Geometries in Ethanol Solvent

Similar to water solvation, we modeled several initial geometries in order to identify the most stable structure. For the explicit solvation method, an ethanol solvent molecule was placed in several different initial geometries for each select adsorbate, and the optimized structure with the lowest energy was considered the most stable structure. When using hybrid solvation (a

combination of the implicit and explicit methods), the optimized structures from the explicit methods were chosen as initial geometries, and we then applied ethanol implicit solvation. Figures S25 to S39 and Tables S24 to S38 show the optimized geometries of adsorbed ethanol oxidation components in ethanol solvent, and the bond lengths of adsorbates.

The implicit solvation method had minimal impact on the adsorbates geometries, as indicated in the appropriate Tables and Figures. The average bond length change using implicit ethanol solvation compared to vacuum was 0.00 Å with a maximum change of 0.01 Å. The maximum and minimum distance changes between the adsorbates and surfaces were 0.06 and 0.00 Å, respectively. With explicit solvation the maximum bond length change within adsorbed species was 0.03 Å, while the average change was 0.01 Å with a standard deviation of 0.01 Å. However, the distance between species and surface changed anywhere from 0.00 to 0.98 Å, with an average change of 0.06 Å. Hybrid solvation led to very similar geometries as explicit solvation; the maximum adsorbate bond length change within adsorbate molecules was 0.04 Å with an average change of 0.01 Å. Moreover, the largest distance change between the species and surface was 0.92 Å, while the average change was 0.06 Å with a standard deviation of 0.16 Å. Intermolecular hydrogen bonds also formed between the adsorbates and the ethanol solvent molecules when using the explicit and hybrid ethanol solvation approaches. When using both solvation models, strong hydrogen bonds formed between ethanol and several adsorbate species (CH_3CH_2OH, CH_3CH_2O, CH_2CH_2O, CH_2OH, CH_2O, CH_3CO, CH_2CO, CHCO, CO, and OH), with an average hydrogen bond length of 1.66 Å. Weaker hydrogen bonds also formed between the ethanol O atom and the H atom of some species (CH_3, CH_2, CH, and CH_3COOH), with an average hydrogen bond length of 2.46 Å. For adsorbed H, the distance between the H atom and ethanol molecule was beyond 3 Å.

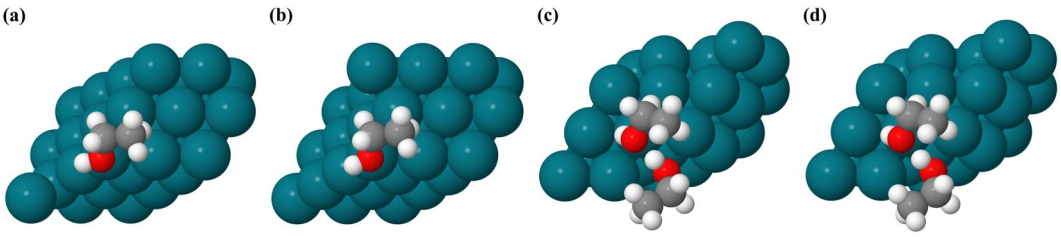

Figure S25: Optimized ethanol structures adsorbed on Rh(111) in (a)vacuum. Also given are structures using (b)implicit, (c)explicit, and (d)hybrid ethanol solvation approaches.

Table S24: Bond lengths of optimized structures of ethanol adsorbed on Rh(111) in various ethanol solvation environments.

Bond Length (Å)				
	vacuum	implicit	explicit	hybrid
C_1-O	1.46	1.47	1.45	1.45
C_1-C_2	1.51	1.51	1.51	1.51
C-H	1.10	1.10	1.10	1.10
O-H	0.98	0.98	0.99	0.99
O-Rh	2.31	2.25	3.29	3.23
H bond(ethanol-ads)	-	-	1.68	1.64

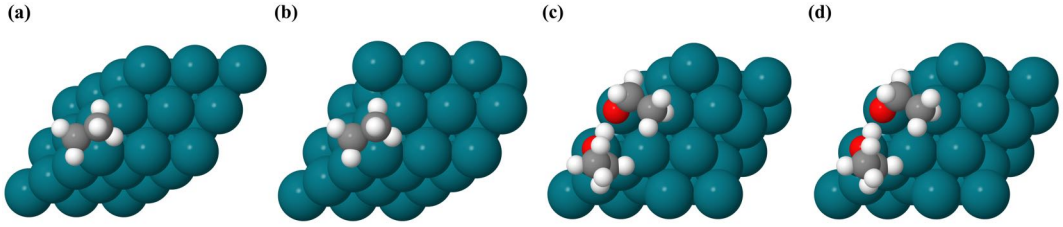

Figure S26: Optimized CH_3CH_2O structures adsorbed on Rh(111) in (a)vacuum. Also given are structures using (b)implicit, (c)explicit, and (d)hybrid ethanol solvation approaches.

Table S25: Bond lengths of optimized structures of CH_3CH_2O adsorbed on Rh(111) in various ethanol solvation environments.

Bond Length (Å)				
	vacuum	implicit	explicit	hybrid
C_1-O	1.44	1.45	1.42	1.42
C_1-C_2	1.51	1.51	1.52	1.52
C-H	1.10	1.10	1.10	1.10
O-Rh	2.17	2.16	2.05	2.04
H bond(ethanol-ads)	-	-	1.41	1.42

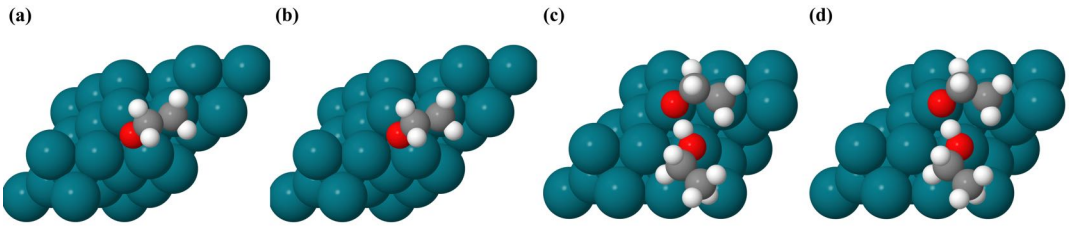

Figure S27: Optimized CH_2CH_2O structures adsorbed on Rh(111) in (a)vacuum. Also given are structures using (b)implicit, (c)explicit, and (d)hybrid ethanol solvation approaches.

Table S26: Bond lengths of optimized structures of CH_2CH_2O adsorbed on Rh(111) in various ethanol solvation environments.

Bond Length (Å)				
	vacuum	implicit	explicit	hybrid
C_1-O	1.45	1.45	1.42	1.41
C_1-C_2	1.52	1.52	1.51	1.51
C-H	1.10	1.10	1.10	1.10
O-Rh_1	2.13	2.12	2.08	2.07
O-Rh_2	2.11	2.11	-	-
C_2-Rh	2.11	2.10	2.10	2.10
H bond(ethanol-ads)	-	-	1.44	1.49

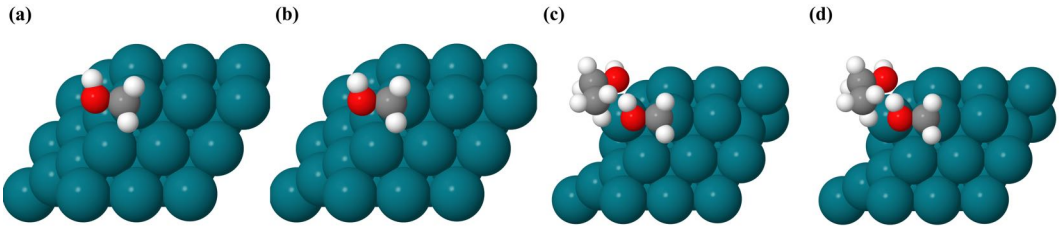

Figure S28: Optimized CH_2OH structures adsorbed on Rh(111) in (a)vacuum. Also given are structures using (b)implicit, (c)explicit, and (d)hybrid ethanol solvation approaches.

Table S27: Bond lengths of optimized structures of CH_2OH adsorbed on Rh(111) in various ethanol solvation environments.

Bond Length (Å)				
	vacuum	implicit	explicit	hybrid
C-O	1.46	1.45	1.44	1.44
C-H	1.10	1.10	1.10	1.10
C-Rh	2.07	2.07	2.08	2.08
O-H	0.99	0.98	1.02	1.03
H bond(ethanol-ads)	-	-	1.60	1.57

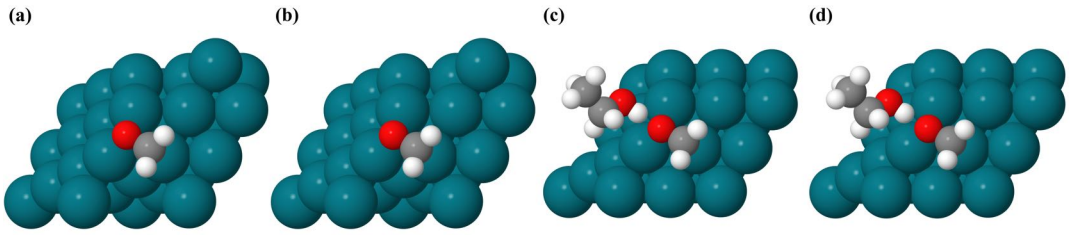

Figure S29: Optimized CH_2O structures adsorbed on Rh(111) in (a)vacuum. Also given are structures using (b)implicit, (c)explicit, and (d)hybrid ethanol solvation approaches.

Table S28: Bond lengths of optimized structures of CH_2O adsorbed on Rh(111) in various ethanol solvation environments.

Bond Length (Å)				
	vacuum	implicit	explicit	hybrid
C-O	1.38	1.39	1.40	1.40
C-H	1.10	1.10	1.10	1.10
O-Rh_1	2.17	2.17	2.21	2.20
O-Rh_2	2.17	2.17	2.23	2.22
C-Rh	2.08	2.08	2.07	2.07
H bond(ethanol-ads)	-	-	1.65	1.66

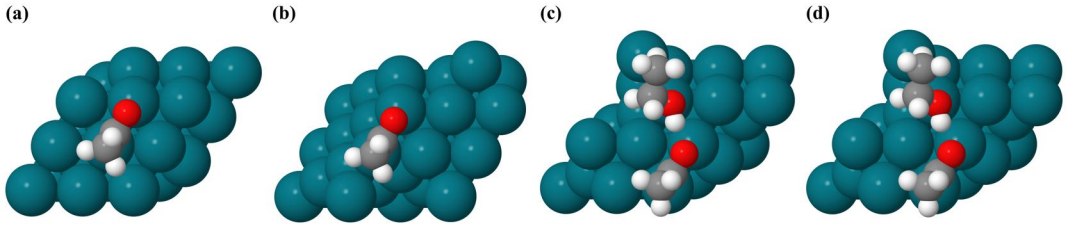

Figure S30: Optimized CH_3CO structures adsorbed on Rh(111) in (a)vacuum. Also given are structures using (b)implicit, (c)explicit, and (d)hybrid ethanol solvation approaches.

Table S29: Bond lengths of optimized structures of CH_3CO adsorbed on Rh(111) in various ethanol solvation environments.

Bond Length (Å)				
	vacuum	implicit	explicit	hybrid
C_1-O	1.26	1.26	1.28	1.28
C_1-C_2	1.50	1.50	1.51	1.50
C-H	1.10	1.10	1.10	1.10
O-Rh	2.16	2.15	2.21	2.19
C_1-Rh	1.96	1.96	1.94	1.94
H bond(ethanol-ads)	-	-	1.81	1.83

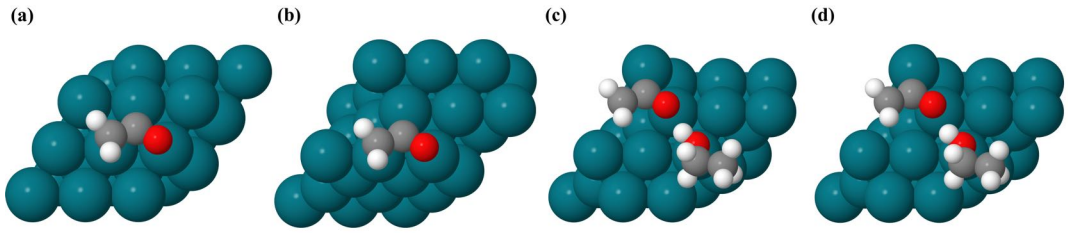

Figure S31: Optimized CH_2CO structures adsorbed on Rh(111) in (a)vacuum. Also given are structures using (b)implicit, (c)explicit, and (d)hybrid ethanol solvation approaches.

Table S30: Bond lengths of optimized structures of CH_2CO adsorbed on Rh(111) in various ethanol solvation environments.

Bond Length (Å)				
	vacuum	implicit	explicit	hybrid
C_1-O	1.29	1.29	1.31	1.31
C_1-C_2	1.44	1.44	1.44	1.44
C-H	1.10	1.10	1.10	1.10
O-Rh	2.11	2.12	2.13	2.13
C_1-Rh_1	2.49	2.49	2.48	2.48
C_1-Rh_2	2.28	2.28	2.28	2.28
C_1-Rh_3	2.05	2.05	2.06	2.06
C_2-Rh	2.17	2.17	-	-
H bond(ethanol-ads)	-	-	1.84	1.87

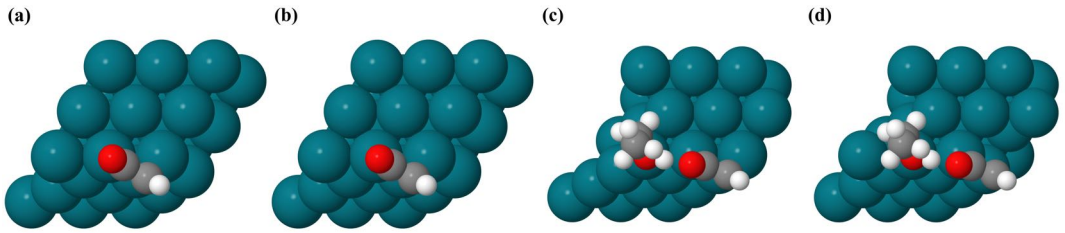

Figure S32: Optimized CH_2CO structures adsorbed on Rh(111) in (a)vacuum. Also given are structures using (b)implicit, (c)explicit, and (d)hybrid ethanol solvation approaches.

Table S31: Bond lengths of optimized structures of CHCO adsorbed on Rh(111) in various ethanol solvation environments.

Bond Length (Å)				
	vacuum	implicit	explicit	hybrid
C_1-O	1.21	1.22	1.24	1.24
C_1-C_2	1.44	1.44	1.44	1.44
C-H	1.10	1.10	1.10	1.10
C_1-Rh	2.05	2.04	2.02	2.01
C_2-Rh	2.06	2.05	2.05	-
H bond(ethanol-ads)	-	-	1.65	1.65

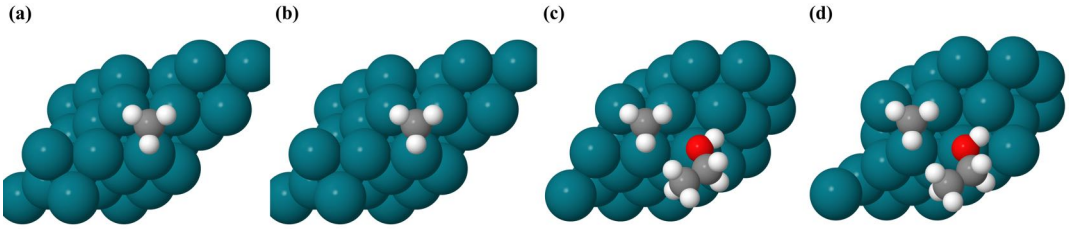

Figure S33: Optimized CH_3 structures adsorbed on Rh(111) in (a)vacuum. Also given are structures using (b)implicit, (c)explicit, and (d)hybrid ethanol solvation approaches.

Table S32: Bond lengths of optimized structures of CH_3 adsorbed on Rh(111) in various ethanol solvation environments.

Bond Length (Å)				
	vacuum	implicit	explicit	hybrid
C-H	1.12	1.12	1.12	1.12
C-Rh_1	2.26	2.25	2.27	2.26
C-Rh_2	2.26	2.25	-	-
C-Rh_3	2.27	2.25	-	-
H bond(ethanol-ads)	-	-	2.78	2.81

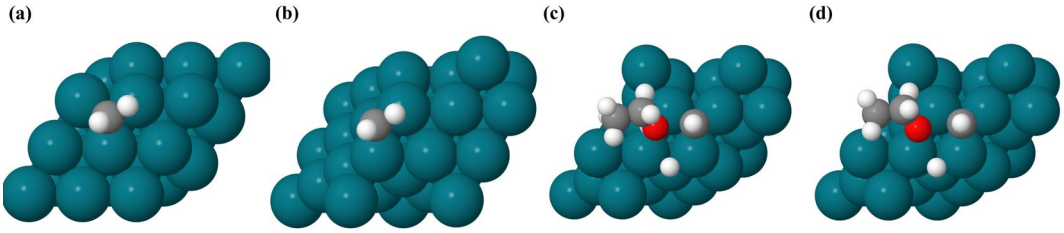

Figure S34: Optimized CH_2 structures adsorbed on Rh(111) in (a)vacuum. Also given are structures using (b)implicit, (c)explicit, and (d)hybrid ethanol solvation approaches.

Table S33: Bond lengths of optimized structures of CH_2 adsorbed on Rh(111) in various ethanol solvation environments.

Bond Length (Å)				
	vacuum	implicit	explicit	hybrid
C-H	1.10	1.10	1.10	1.10
C-Rh_1	2.03	2.03	1.99	1.99
C-Rh_2	2.03	2.03	1.99	1.98
C-Rh_3	2.16	2.15	1.97	1.97
H bond(ethanol-ads)	-	-	2.46	2.66

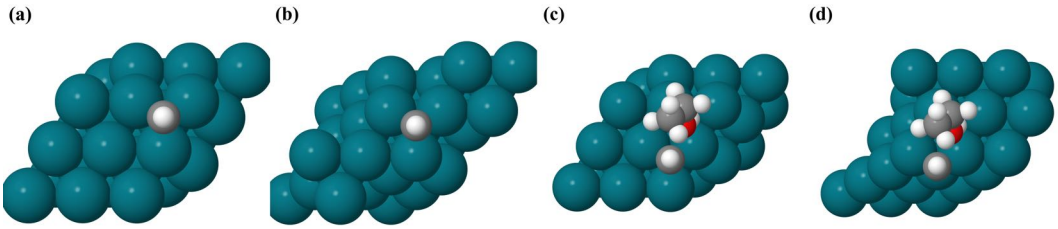

Figure S35: Optimized CH structures adsorbed on Rh(111) in (a)vacuum. Also given are structures using (b)implicit, (c)explicit, and (d)hybrid ethanol solvation approaches.

Table S34: Bond lengths of optimized structures of CH adsorbed on Rh(111) in various ethanol solvation environments.

Bond Length (Å)				
	vacuum	implicit	explicit	hybrid
C-H	1.10	1.10	1.10	1.10
C-Rh_1	1.98	1.98	1.98	1.98
C-Rh_2	1.98	1.98	1.98	1.98
C-Rh_3	1.98	1.98	1.98	1.98
H bond(ethanol-ads)	-	-	2.41	2.44

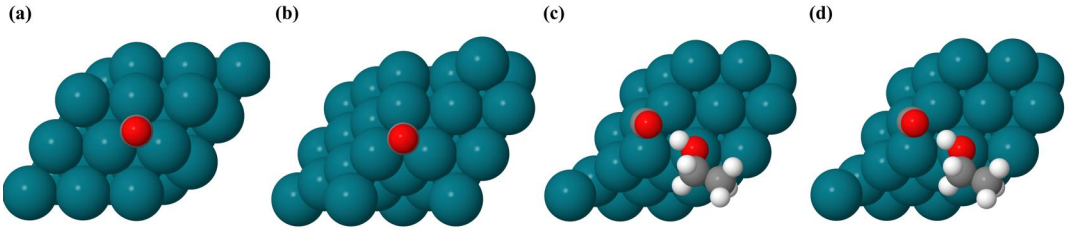

Figure S36: Optimized CO structures adsorbed on Rh(111) in (a)vacuum. Also given are structures using (b)implicit, (c)explicit, and (d)hybrid ethanol solvation approaches.

Table S35: Bond lengths of optimized structures of CO adsorbed on Rh(111) in various ethanol solvation environments.

Bond Length (Å)				
	vacuum	implicit	explicit	hybrid
C-O	1.20	1.20	1.22	1.22
C-Rh_1	2.10	2.10	2.08	2.07
C-Rh_2	2.10	2.10	2.08	2.07
C-Rh_3	2.10	2.10	2.08	2.07
H bond(ethanol-ads)	-	-	1.89	1.93

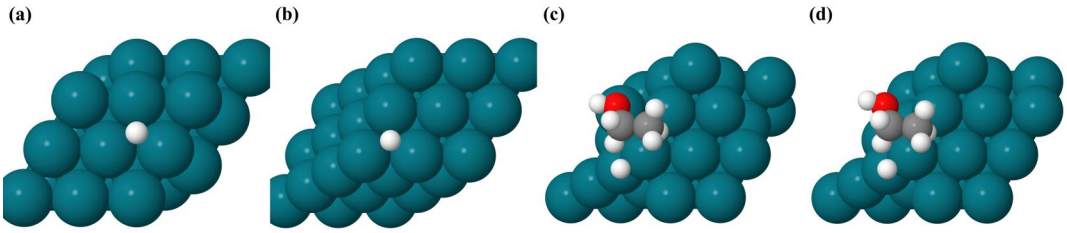

Figure S37: Optimized H structures adsorbed on Rh(111) in (a)vacuum. Also given are structures using (b)implicit, (c)explicit, and (d)hybrid ethanol solvation approaches.

Table S36: Bond lengths of optimized structures of H adsorbed on Rh(111) in various ethanol solvation environments.

Bond Length (Å)				
	vacuum	implicit	explicit	hybrid
H-Rh_1	1.86	1.86	1.86	1.86
H-Rh_2	1.86	1.86	1.86	1.86
H-Rh_3	1.86	1.86	1.86	1.86

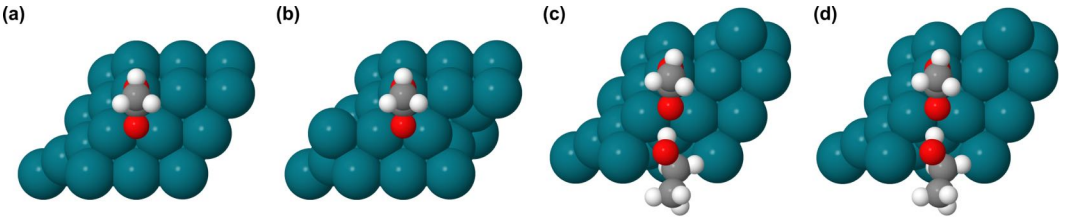

Figure S38: Optimized CH_3COOH structures adsorbed on Rh(111) in (a)vacuum. Also given are structures using (b)implicit, (c)explicit, and (d)hybrid ethanol solvation approaches.

Table S37: Bond lengths of optimized structures of CH_3COOH adsorbed on Rh(111) in various ethanol solvation environments.

Bond Length (Å)				
	vacuum	implicit	explicit	hybrid
C_1-O_1	1.25	1.25	1.25	1.25
C_1-O_2	1.32	1.32	1.33	1.33
O_2-H	1.02	1.02	1.03	1.03
C-H	1.1	1.09	1.09	1.09
C_1-C_2	1.5	1.49	1.5	1.49
O_1-Rh	2.17	2.15	2.18	2.15
H bond(ethanol-ads)	-	-	2.07	2.02

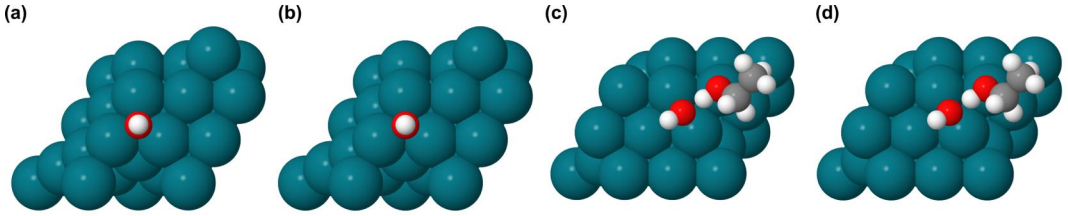

Figure S39: Optimized OH structures adsorbed on Rh(111) in (a)vacuum. Also given are structures using (b)implicit, (c)explicit, and (d)hybrid ethanol solvation approaches.

Table S38: Bond lengths of optimized structures of OH adsorbed on Rh(111) in various ethanol solvation environments.

Bond Length (Å)				
	vacuum	implicit	explicit	hybrid
O-H_1	0.97	0.98	0.98	0.98
O-Rh_1	2.16	2.14	2.20	2.18
O-Rh_2	2.17	2.15	2.19	2.18
O-Rh_3	2.17	2.15	-	-
H bond(ethanol-ads)	-	-	1.56	1.55

10 Summary of Ethanol Solvent Energies

All the adsorption and reaction energies for the various ethanol solvent results are given in Tables S39 and S40.

Table S39: Adsorption free energies on Rh(111) in ethanol solvent of species relevant to ethanol oxidation. Results are shown in vacuum and with various solvation models.

ΔG_{ads} (eV)				
	vacuum	implicit	explicit	hybrid
$*CH_3CH_2OH$	0.12	0.13	-0.03	0.14
$*CH_3CH_2O$	-1.61	-1.55	-1.69	-1.52
$*CH_2CH_2O$	-0.67	-0.62	-0.79	-0.64
$*CH_2OH$	-1.44	-1.44	-1.62	-1.42
$*CH_2O$	-0.29	-0.20	-0.37	-0.19
$*CH_3CO$	-1.79	-1.76	-1.71	-1.60
$*CH_2CO$	-0.79	-0.78	-0.78	-0.67
$*CHCO$	-2.91	-2.85	-3.23	-3.01
$*CH_3$	-1.33	-1.38	-1.22	-1.23
$*CH_2$	-3.60	-3.62	-3.96	-3.87
$*CH$	-6.17	-6.14	-6.06	-5.92
$*CO$	-1.45	-1.51	-1.59	-1.54
$*H$	-0.39	-0.39	-0.28	-0.29
$*CH_3COOH$	-0.03	0.06	0.08	0.29
$*OH$	-2.57	-2.56	-2.70	-2.55

Table S40: Reaction free energies on Rh(111) in ethanol solvent of species relevant to ethanol oxidation. Results are shown in vacuum and with various solvation models.

ΔG_{rxn} (eV)				
	vacuum	implicit	explicit	hybrid
$*CH_3CH_2OH + * \rightarrow *CH_3 + *CH_2OH$	0.38	0.32	0.46	0.47
$*CH_3CH_2O + * \rightarrow *CH_3 + *CH_2O$	0.28	0.25	0.40	0.38
$*CH_2CH_2O + * \rightarrow *CH_2 + *CH_2O$	-0.13	-0.17	-0.44	-0.38
$*CH_3CO + * \rightarrow *CH_3 + *CO$	-0.43	-0.48	-0.56	-0.51
$*CH_2CO + * \rightarrow *CH_2 + *CO$	-0.80	-0.85	-1.31	-1.23
$*CHCO + * \rightarrow *CH + *CO$	-1.06	-1.06	-0.77	-0.70
$*CH_3CO + * \rightarrow *CH_2CO + *H$	0.10	0.10	0.13	0.16
$*CH_2CO + * \rightarrow *CHCO + *H$	-0.35	-0.39	-0.57	-0.55
$*CH_3CO + *OH \rightarrow *CH_3COOH + *$	-0.13	-0.08	0.02	-0.03

11 Further Details on Adsorption and Reaction Enthalpies

When calculating $\Delta H_{rxn-free-species}$ with vacuum, explicit and explicit+ solvation methods we used gas-phase (vacuum) enthalpies of lone molecules. When calculating $\Delta H_{rxn-free-species}$ with implicit and hybrid solvation methods, the enthalpies of free molecules were calculated from lone molecules under implicit solvation. Table S41 shows that enthalpies of vacuum and implicitly-solvated molecules were very similar. The average difference was only 0.11 eV. Tables S42 and S43 provide $\Delta\Delta H_{ads}$ and $\Delta H_{rxn-surf}$ values for reactions using each of the solvation methods.

Table S41: Calculated enthalpies of isolated molecules in vacuum or implicit solvation.

$H_{free-species}$ (eV)		
	vacuum	implicit
CH_3CH_2OH	-44.46	-44.65
CH_3CH_2O	-39.17	-39.32
CH_2CH_2O	-36.29	-36.41
CH_2OH	-23.40	-23.60
CH_2O	-21.18	-21.35
CH_3CO	-32.64	-32.77
CH_2CO	-29.84	-29.94
CHCO	-24.39	-24.49
CH_3	-17.13	-17.14
CH_2	-11.39	-11.42
CH	-5.59	-5.77
CO	-14.44	-14.45
H	-1.00	-0.98

Table S42: $\Delta\Delta H_{ads}$ for chemical reactions involved in C-C and C-H bond scission reactions.

$\Delta\Delta H_{ads}$ (eV)							
No.	Reaction	vacuum	implicit	explicit	hybrid	explicit+	bond-additivity
1	$*CH_3CH_2OH + * \rightarrow *CH_3 + *CH_2OH$	-3.52	-3.58	-3.62	-3.58	-3.41	-2.56
2	$*CH_3CH_2O + * \rightarrow *CH_3 + *CH_2O$	-0.49	-0.50	-0.65	-0.52	-0.66	0.67
3	$*CH_2CH_2O + * \rightarrow *CH_2 + *CH_2O$	-3.75	-3.72	-3.62	-3.64	-3.83	-2.74
4	$*CH_3CO + * \rightarrow *CH_3 + *CO$	-1.39	-1.56	-1.52	-1.61	-1.55	-0.23
5	$*CH_2CO + * \rightarrow *CH_2 + *CO$	-4.64	-4.76	-4.71	-4.80	-4.69	-3.61
6	$*CHCO + * \rightarrow *CH + *CO$	-5.22	-5.22	-5.13	-5.17	-5.09	-4.44
7	$*CH_3CO + * \rightarrow *CH_2CO + *H$	-1.60	-1.63	-1.95	-1.93	-1.96	-0.46
8	$*CH_2CO + * \rightarrow *CHCO + *H$	-4.55	-4.61	-4.90	-4.93	-4.91	-3.50

Table S43: $\Delta H_{rxn-surf}$ for chemical reactions involved in C-C and C-H bond scission reactions.

		$\Delta H_{rxn-surf}$ (eV)					
No.	Reaction	vacuum	implicit	explicit	hybrid	explicit+	bond-additivity
1	$*CH_3CH_2OH + * \rightarrow *CH_3 + *CH_2OH$	0.41	0.33	0.31	0.34	0.52	1.37
2	$*CH_3CH_2O + * \rightarrow *CH_3 + *CH_2O$	0.37	0.32	0.21	0.30	0.20	1.52
3	$*CH_2CH_2O + * \rightarrow *CH_2 + *CH_2O$	-0.02	-0.07	0.10	0.01	-0.10	0.98
4	$*CH_3CO + * \rightarrow *CH_3 + *CO$	-0.33	-0.38	-0.46	-0.43	-0.49	0.83
5	$*CH_2CO + * \rightarrow *CH_2 + *CO$	-0.63	-0.68	-0.70	-0.73	-0.69	0.40
6	$*CHCO + * \rightarrow *CH + *CO$	-0.96	-0.95	-0.87	-0.89	-0.83	-0.18
7	$*CH_3CO + * \rightarrow *CH_2CO + *H$	0.20	0.21	-0.14	-0.08	-0.16	1.34
8	$*CH_2CO + * \rightarrow *CHCO + *H$	-0.10	-0.15	-0.46	-0.46	-0.46	0.95

References

(1) Blöchl, P. E. Projector augmented-wave method. *Physical Review B* **1994**, *50*, 17953–17979.

(2) G. Kresse and D. Joubert, From ultrasoft pseudopotentials to the projector augmented-wave method. *Physical Review B - Condensed Matter and Materials Physics* **1999**, *59*, 1758–1775.

(3) Michel, C.; Göltl, F.; Sautet, P. Early stages of water/hydroxyl phase generation at transition metal surfaces - Synergetic adsorption and O-H bond dissociation assistance. *Physical Chemistry Chemical Physics* **2012**, *14*, 15286–15290.

(4) Motobayashi, K.; Árnadóttir, L.; Matsumoto, C.; Stuve, E. M.; Jónsson, H.; Kim, Y.; Kawai, M. Adsorption of Water Dimer on Platinum(111): Identification of the -OH···Pt Hydrogen Bond. *ACS Nano* **2014**, *8*, 11583–11590.

(5) Árnadóttir, L.; Stuve, E. M.; Jónsson, H. Adsorption of water monomer and clusters on platinum(111) terrace and related steps and kinks: I. Configurations, energies, and hydrogen bonding. *Surface Science* **2010**, *604*, 1978–1986.

(6) Meng, S.; Wang, E. G.; Gao, S. Water adsorption on metal surfaces: A general picture from density functional theory studies. *Phys. Rev. B* **2004**, *69*, 195404.

(7) Choi, Y. M.; Liu, P. Mechanism of ethanol synthesis from syngas on Rh(111). *Journal of the American Chemical Society* **2009**, *131*, 13054–13061.

(8) Li, M.; Guo, W.; Jiang, R.; Zhao, L.; Lu, X.; Zhu, H.; Fu, D.; Shan, H. Density functional study of ethanol decomposition on Rh(111). *Journal of Physical Chemistry C* **2010**, *114*, 21493–21503.

(9) Michel, C.; Auneau, F.; Delbecq, F.; Sautet, P. C-H versus O-H bond dissociation for

alcohols on a Rh(111) Surface: A strong assistance from hydrogen bonded neighbors. *ACS Catalysis* **2011**, *1*, 1430–1440.

(10) Mavrikakis, M.; Rempel, J.; Greeley, J.; Hansen, L. B.; Nørskov, J. K.; Rempel, . J. Atomic and molecular adsorption on Rh(111) Structure sensitivity in the CO oxidation on rhodium: Effect of adsorbate coverages on oxidation kinetics on Molecular and dissociative chemisorption of NO on palladium and rhodium (100) and (111) surfaces: A den. *The Journal of Chemical Physics* **2002**, *117*, 9901.

(11) Pozzo, M.; Carlini, G.; Rosei, R.; Alfè, D. Comparative study of water dissociation on Rh(111) and Ni(111) studied with first principles calculations. *Journal of Chemical Physics* **2007**, *126*, 12.

(12) Jiang, R.; Guo, W.; Li, M.; Zhu, H.; Zhao, L.; Lu, X.; Shan, H. Methanol dehydrogenation on Rh(1 1 1): A density functional and microkinetic modeling study. *Journal of Molecular Catalysis A: Chemical* **2011**, *344*, 99–110.

(13) Zhao, X.; Zhang, R.; Wang, Q.; Li, D.; Wang, B.; Ling, L. Source and major species of CHx (x = 1-3) in acetic acid synthesis from methane-syngas on Rh catalyst: A theoretical study. *RSC Advances* **2014**, *4*, 58631–58642.

(14) Choi, Y.; Liu, P. Understanding of ethanol decomposition on Rh(1 1 1) from density functional theory and kinetic Monte Carlo simulations. Catalysis Today. 2011; pp 64–70.

(15) Xie, T.; Sarupria, S.; Getman, R. B. A DFT and MD study of aqueous-phase dehydrogenation of glycerol on Pt(1 1 1): comparing chemical accuracy versus computational expense in different methods for calculating aqueous-phase system energies. *Molecular Simulation* **2017**, *43*, 370–378.

(16) Xie, T.; Bodenschatz, C. J.; Getman, R. B. Insights into the roles of water on the

aqueous phase reforming of glycerol. *Reaction Chemistry and Engineering* **2019**, *4*, 383–392.

(17) Wang, S.; Temel, B.; Shen, J.; Jones, G.; Grabow, L. C.; Studt, F.; Bligaard, T.; Abild-Pedersen, F.; Christensen, C. H.; Nørskov, J. K. Universal Brønsted-Evans-Polanyi relations for C-C, C-O, C-N, N-O, N-N, and O-O dissociation reactions. *Catalysis Letters* **2011**, *141*, 370–373.

(18) Wang, S. et al. Universal transition state scaling relations for (de)hydrogenation over transition metals. *Physical Chemistry Chemical Physics* **2011**, *13*, 20760–20765.

(19) Schweitzer, B.; Steinmann, S. N.; Michel, C. Can microsolvation effects be estimated from vacuum computations? A case-study of alcohol decomposition at the H 2 O/Pt(111) interface. *Physical Chemistry Chemical Physics* **2019**, *21*, 5368–5377.

(20) Akinola, J.; Barth, I.; Goldsmith, B. R.; Singh, N. Adsorption Energies of Oxygenated Aromatics and Organics on Rhodium and Platinum in Aqueous Phase. *ACS Catalysis* **2020**, *10*, 4929–4941.

(21) Singh, N.; Campbell, C. T. A Simple Bond-Additivity Model Explains Large Decreases in Heats of Adsorption in Solvents Versus Gas Phase: A Case Study with Phenol on Pt(111) in Water. *ACS Catalysis* **2019**, *9*, 8116–8127.

(22) Lew, W.; Crowe, M. C.; Karp, E.; Campbell, C. T. Energy of Molecularly Adsorbed Water on Clean Pt(111) and Pt(111) with Coadsorbed Oxygen by Calorimetry. *The Journal of Physical Chemistry C* **2011**, *115*, 9164–9170.

(23) Le, J.; Cuesta, A.; Cheng, J. The structure of metal-water interface at the potential of zero charge from density functional theory-based molecular dynamics. *Journal of Electroanalytical Chemistry* **2018**, *819*, 87–94.

(24) Osborne, N.; Stimson, H.; Ginnings, D. Measurements of heat capacity and heat of vaporization of water in the range 0 degrees to 100 degrees C. *Journal of Research of the National Bureau of Standards* **1939**, *23*, 197.

(25) Rumptz, J. R.; Campbell, C. T. Adhesion Energies of Solvent Films to Pt(111) and Ni(111) Surfaces by Adsorption Calorimetry. *ACS Catalysis* **2019**, *9*, 11819–11825.

(26) Vorotnikov, V.; Wang, S.; Vlachos, D. G. Group additivity for estimating thermochemical properties of furanic compounds on Pd(111). *Industrial and Engineering Chemistry Research* **2014**, *53*, 11929–11938.

(27) Gu, G. H.; Schweitzer, B.; Michel, C.; Steinmann, S. N.; Sautet, P.; Vlachos, D. G. Group Additivity for Aqueous Phase Thermochemical Properties of Alcohols on Pt(111). *The Journal of Physical Chemistry C* **2017**, *121*, 21510–21519.

(28) Cramer, C. J. *Essentials of Computational Chemistry:Theories and Models, 2nd Edition*; Wiley, 2004.

(29) Heit, Y. N.; Beran, G. J. How important is thermal expansion for predicting molecular crystal structures and thermochemistry at finite temperatures? *Acta Crystallographica Section B: Structural Science, Crystal Engineering and Materials* **2016**, *72*, 514–529.

(30) Alfonso, D. R. Computational Investigation of FeS2 Surfaces and Prediction of Effects of Sulfur Environment on Stabilities. *The Journal of Physical Chemistry C* **2010**, *114*, 8971–8980.

(31) Reuter, K.; Scheffler, M. Composition, structure, and stability of (formula presented) as a function of oxygen pressure. *Physical Review B - Condensed Matter and Materials Physics* **2002**, *65*, 1–11.

(32) Hensen, U.; Gräter, F.; Henchman, R. H. Macromolecular entropy can be accurately

computed from force. *Journal of Chemical Theory and Computation* **2014**, *10*, 4777–4781.

(33) Sander, R. Compilation of Henry's law constants (version 4.0) for water as solvent. *Atmospheric Chemistry and Physics* **2015**, *15*, 4399–4981.

(34) He, R.; Kusaka, H.; Mavrikakis, M.; Dumesic, J. A. Microcalorimetric, infrared spectroscopic and DFT studies of CO adsorption on Rh and Rh–Te catalysts. *Journal of Catalysis* **2003**, *217*, 209–221.

(35) Klötzer, B.; Unterberger, W.; Hayek, K. Adsorption and hydrogenation of CO on Pd(1 1 1) and Rh(1 1 1) modified by subsurface vanadium. *Surface Science* **2003**, *532-535*, 142–147.

(36) Thiel, P. A.; Williams, E. D.; Yates, J. T.; Weinberg, W. H. The chemisorption of Co on Rh(111). *Surface Science* **1979**, *84*, 54–64.